DEPARTMENT OF COMMERCE
LEWIS L. STRAUSS, Secretary

WEATHER BUREAU
F. W. REICHELDERFER, Chief

MONTHLY WEATHER REVIEW

JAMES E. CASKEY, JR., Editor

Volume 87
Number 4

APRIL 1959

Closed June 15, 1959
Issued July 15, 1959

THE EFFECTS OF VERTICAL VORTICITY ADVECTION AND TURNING OF THE VORTEX TUBES IN HEMISPHERIC FORECASTS WITH A TWO-LEVEL MODEL

G. 'ARNASON and L. P. CARSTENSEN, U.S. Weather Bureau [1]

Joint Numerical Weather Prediction Unit, Suitland, Md.

[Manuscript received December 10, 1958; revised March 9, 1959]

ABSTRACT

A 2-parameter forecasting model which includes the effects of vertical vorticity advection and turning of the vortex tubes is briefly described. Contributions of the above-mentioned terms are discussed and an example is presented.

The importance of consistent truncation over a large grid is pointed out.

1. INTRODUCTION

In the summer of 1957, the Joint Numerical Weather Prediction Unit (JNWP) changed from an IBM 701 to an IBM 704 electronic computer. Because of the higher capacity of the latter, the forecast area was extended to cover the Northern Hemisphere north of latitude 13°. Rather than recode the two-level, geostrophic model in use prior to the change of machine, it was decided to test a slightly more elaborate two-level model in the hope of improving the forecasts. This model was designed by Lt. Col. Philip D. Thompson, then Chief of the Research and Development Section of JNWP [1].

In testing this model some difficulties were encountered which had not been fully anticipated. These difficulties were due in part to attempted simple extension of the model from the one previously used, but more importantly to the increased importance of accumulated systematic small errors over a large grid.

This report is concerned mainly with consequences resulting from including the vertical advection of vorticity and the twisting terms in the prognostic equations.

[1] Present affiliation: Navy Numerical Weather Problems Group, U.S. Naval Postgraduate School, Monterey, Calif.

2. DESCRIPTION OF THE MODEL

The model's information levels are at 400 and 800 mb. As is customary, the ω-profile $\left(\omega=\frac{dp}{dt}\right)$ is assumed to have a smooth shape, and is for this particular model symmetrical in the vertical about $p=600$ mb. and zero for $p=200$ and $p=1000$ mb.

Application of the vorticity equation to the information levels results in two predictive equations:

$$\frac{\partial \eta_1}{\partial t}+\mathbf{v}_1\cdot\nabla\eta_1-\eta_1\frac{\partial \omega_1}{\partial p}+\omega_1\frac{\partial \eta_1}{\partial p}+\mathbf{k}\cdot\nabla\omega_1\times\frac{\partial \mathbf{v}_1}{\partial p}=0 \qquad (1)$$

$$\frac{\partial \eta_2}{\partial t}+\mathbf{v}_2\cdot\nabla\eta_2-\eta_2\frac{\partial \omega_2}{\partial p}+\omega_2\frac{\partial \eta_2}{\partial p}+\mathbf{k}\cdot\nabla\omega_2\times\frac{\partial \mathbf{v}_2}{\partial p}=0 \qquad (2)$$

where the subscripts 1 and 2 refer to 400 and 800 mb., respectively; notations are conventional.

We define the new variables

$$\eta^1=\frac{1}{2}(\eta_1-\eta_2);\ \mathbf{v}^1=\frac{1}{2}(\mathbf{v}_1-\mathbf{v}_2)$$

$$\bar{\eta}=\frac{1}{2}(\eta_1+\eta_2);\ \bar{\mathbf{v}}=\frac{1}{2}(\mathbf{v}_1+\mathbf{v}_2). \qquad (3)$$

Addition and subtraction of (1) and (2), utilizing (3), result in

$$\frac{\partial\bar{\eta}}{\partial t}+\bar{\mathbf{v}}\cdot\nabla\bar{\eta}+\mathbf{v}^1\cdot\nabla\eta^1-\frac{1}{2}\left(\eta_1\frac{\partial\omega_1}{\partial p}+\eta_2\frac{\partial\omega_2}{\partial p}\right)$$

$$+\frac{1}{2}\left(\omega_1\frac{\partial\eta_1}{\partial p}+\omega_2\frac{\partial\eta_2}{\partial p}\right)+\frac{1}{2}\mathbf{k}\cdot\left(\nabla\omega_1\times\frac{\partial\mathbf{v}_1}{\partial p}+\nabla\omega_2\times\frac{\partial\mathbf{v}_2}{\partial p}\right)=0$$

$$\frac{\partial\eta^1}{\partial t}+\bar{\mathbf{v}}\cdot\nabla\eta^1+\mathbf{v}^1\cdot\nabla\bar{\eta}-\frac{1}{2}\left(\eta_1\frac{\partial\omega_1}{\partial p}-\eta_2\frac{\partial\omega_2}{\partial p}\right)$$

$$+\frac{1}{2}\left(\omega_1\frac{\partial\eta_1}{\partial p}-\omega_2\frac{\partial\eta_2}{\partial p}\right)+\frac{1}{2}\mathbf{k}\cdot\left(\nabla\omega_1\times\frac{\partial\mathbf{v}_1}{\partial p}-\nabla\omega_2\times\frac{\partial\mathbf{v}_2}{\partial p}\right)=0.$$

These equations are simplified when we observe that $\omega_1=\omega_2=A\omega_{600}$ where the proportionality factor A is assumed to be less than unity, and that the model can not distinguish between the p-derivatives of $\mathbf{v}$ and η at the two information levels. As a further step toward simplification, the derivatives with respect to p are replaced by finite differences as follows:

$$\frac{\partial\omega_1}{\partial p}=-\frac{\partial\omega_2}{\partial p}=\frac{\omega}{P},\quad \frac{\partial\eta_1}{\partial p}=\frac{\partial\eta_2}{\partial p}=-\frac{2\eta^1}{P},\quad \frac{\partial\mathbf{v}_1}{\partial p}=\frac{\partial\mathbf{v}_2}{\partial p}=-\frac{2\mathbf{v}^1}{P} \tag{4}$$

Where $P=400$ mb., and ω refers to the 600-mb. surface.

The prediction equations for $\bar{\eta}$ and η^1 now take the form:

$$\frac{\partial\bar{\eta}}{\partial t}+\bar{\mathbf{v}}\cdot\nabla\bar{\eta}+\mathbf{v}^1\cdot\nabla\eta^1-\frac{\omega}{P}\eta^1-\frac{2A\omega}{P}\eta^1-\frac{2A}{P}\mathbf{k}\cdot\nabla\omega\times\mathbf{v}^1=0 \tag{5}$$

$$\frac{\partial\eta^1}{\partial t}+\bar{\mathbf{v}}\cdot\nabla\eta^1+\mathbf{v}^1\cdot\nabla\bar{\eta}-\frac{\omega\bar{\eta}}{P}=0. \tag{6}$$

It is pointed out that the fourth term in (5), resulting from the divergence terms of (1) and (2), is of the same form and magnitude as the fifth term in (5), which is the contribution of the vertical advection of vorticity. This implies that if the vertical advection and twisting terms were omitted from the vorticity equation, one should approximate the divergence term in such a way that similar terms are not introduced. As will appear later, this is of some importance for the vorticity balance.

It follows from the symmetry imposed upon the ω-distribution that the wind vector $\bar{\mathbf{v}}$ is divergence-free and can therefore be derived from a stream function $\bar{\psi}$. This is accomplished by solving the balance equation.

In deriving the differential wind and vorticity $\mathbf{v}^1$ and η^1, respectively, the geostrophic approximation is invoked, leading to the expressions:

$$\mathbf{v}^1=\frac{g}{2f}\mathbf{k}\times\nabla h;\quad \eta^1=\frac{g}{2f}\nabla^2 h \tag{7}$$

where h is the thickness of the layer 800–400 mb. Since

$$\bar{\mathbf{v}}=\mathbf{k}\times\nabla\bar{\psi}\quad\text{and}\quad\bar{\eta}=\nabla^2\bar{\psi}+f, \tag{8}$$

the two prediction equations (5) and (6) contain the three unknowns $\bar{\psi}$, h, and ω. The third equation needed for making the system of equations complete is the adiabatic equation, applied at 600 mb.,

$$\frac{\partial h}{\partial t}+\bar{\mathbf{v}}\cdot\nabla h-\frac{\sigma^2}{gP}\omega=0 \tag{9}$$

where

$$\sigma^2=-\frac{p^2}{\rho\Theta}\frac{\partial\Theta}{\partial p} \tag{10}$$

and ρ is the density and Θ the potential temperature.

Utilizing the relations (7), (8), and (9), we may write the predictive equations (5) and (6) as follows:

$$\frac{\partial}{\partial t}\nabla^2\bar{\psi}+J(\bar{\psi},\bar{\eta})+\frac{g}{2f}J\left(h,\frac{g}{2f}\nabla^2 h\right)$$

$$-\frac{1+2A}{2}\frac{g\omega}{fP}\nabla^2 h-\frac{gA}{fP}\nabla\omega\cdot\nabla h=0 \tag{11}$$

$$\left(\nabla^2-\frac{2f\bar{\eta}}{\sigma^2}\right)\frac{\partial h}{\partial t}-\frac{2f\bar{\eta}}{\sigma^2}J(\bar{\psi},h)+fJ\left(\bar{\psi},\frac{1}{f}\nabla^2 h\right)+J(h,\bar{\eta})=0. \tag{12}$$

In solving the complete system (9), (11), and (12), one proceeds as follows:

1. solve equation (12) for $\partial h/\partial t$ and extrapolate in time;
2. compute ω from (9), using $\partial h/\partial t$ from step 1;
3. solve (11) for $\bar{\psi}$ at time $t+\Delta t$;
4. repeat the steps 1 to 3.

It can be disputed whether it is worth while including small terms like the twisting and vertical advection terms in such a crude model. As already mentioned, the model cannot distinguish between the vertical advections at the two information levels and the same applies to the twisting term.

In testing the model, however, it was decided to study the effects of the various terms in equation (11), and as a result three versions of (11) were dealt with; these are:

1. Equation (11) is replaced by

$$\frac{\partial}{\partial t}\nabla^2\bar{\psi}+J(\bar{\psi},\bar{\eta})-\frac{g\omega}{fP}\nabla^2 h=0 \tag{13}$$

i.e., the third and fifth terms in (11) have been omitted and A has been set equal to ½;

2. Equation (11) is replaced by

$$\frac{\partial}{\partial t}\nabla^2\bar{\psi}+J(\bar{\psi},\bar{\eta})+\frac{g}{2f}J\left(h,\frac{g}{2f}\nabla^2 h\right)-\frac{2}{3}\frac{g\omega}{fP}\nabla^2 h=0 \tag{14}$$

i.e., the twisting has been omitted;

3. Equation (11) is replaced by

$$\frac{\partial}{\partial t}\nabla^2\bar{\psi}+J(\bar{\psi},\bar{\eta})+\frac{g}{2f}J\left(h,\frac{g}{2f}\nabla^2 h\right)$$

$$-\frac{g\omega}{fP}\nabla^2 h-\frac{g}{fP}\nabla\omega\cdot\nabla h=0 \quad (15)$$

i.e., the term $\frac{1}{2}\frac{g\omega}{fP}\nabla^2 h$, originating from the divergence terms in (1) and (2), has been neglected, and A set equal to unity. The latter is inconsistent with the assumption that A be less than unity, but this inconsistency is not of any significance.

3. COMMENTS ON VORTICITY BALANCE AND FICTITIOUS SOURCES OF VORTICITY

Omitting friction, we may write the vorticity equation as follows:

$$\frac{\partial\zeta}{\partial t}+\text{div}\,\eta\,\mathbf{v}+\mathbf{k}\cdot\nabla\times\omega\frac{\partial\mathbf{v}}{\partial p}=0. \quad (16)$$

Integration of (16) over an area A of a pressure surface bounded by a curve C gives

$$\frac{\partial\bar{\zeta}}{\partial t}+\frac{1}{A}\int_A \text{div}\,\eta\mathbf{v}dA+\frac{1}{A}\int_A\nabla\times\omega\frac{\partial\mathbf{v}}{\partial p}\cdot\mathbf{k}dA=$$

$$\frac{\partial\bar{\zeta}}{\partial t}+\frac{1}{A}\int_c\eta\mathbf{v}\cdot\mathbf{n}dC+\frac{1}{A}\int_c\omega\frac{\partial\mathbf{v}}{\partial p}\cdot\mathbf{t}dC=0 \quad (17)$$

where dA is an area element, $\mathbf{n}$ a unit vector normal to the unit vector $\mathbf{t}$ which in turn is tangential to the curve C of which dC is an element; $\mathbf{t}$, $\mathbf{n}$, and $\mathbf{k}$ form a right-hand system.

We substitute for $\mathbf{v}$ from

$$\mathbf{v}=\mathbf{k}\times\nabla\psi+\nabla X \quad (18)$$

into (17) which takes the form

$$\frac{\partial\bar{\zeta}}{\partial t}+\frac{1}{A}\left[\int_c\eta d\psi+\int_c\eta\nabla X\cdot\mathbf{n}ds+\int_c\omega\frac{\partial\mathbf{v}}{\partial p}\cdot d\mathbf{r}\right]=0 \quad (19)$$

Thus the mean vorticity $\bar{\zeta}$ may be changed as follows:

(a) by advection of vorticity across the lateral boundaries by the divergence-free part of the wind;

(b) by vorticity advection across the lateral boundaries by the non-rotational part of the wind and due to its divergence ($\nabla X\cdot\nabla\eta$ and $\eta\text{div}\mathbf{v}$);

(c) vertical advection of circulation along the boundary curve C.

If we impose the boundary condition $\mathbf{v}\cdot\mathbf{n}=0$ and $\omega=0$, i.e., if the system is closed, the mean vorticity is independent of time. Hence, as long as the vorticity equation is not approximated there are no vorticity sources. This is of interest to bear in mind when dealing with simple models where approximations are inevitable. For example, in omitting the advection of vorticity by the non-rotational part of the wind in the vorticity equation and keeping the divergence term, a false vorticity source may thereby be introduced, upsetting the vorticity balance. This argument applies also to the twisting and vertical advection terms in the vorticity equation; retaining one of them and omitting the other introduces a spurious vorticity source.

As will be shown later, this introduction of spurious vorticity sources is not to be taken lightly when dealing with forecasts over a large area. For a hemispheric grid it introduces a large-scale error devastating for the usefulness of the forecast.

4. DISCUSSION OF THE FORECASTS

All forecasts discussed here were made using the JNWP octagonal grid which covers the Northern Hemisphere north of latitude 13°.

In investigating the performance of the models, the contributions of certain of the terms of the prediction equation for $\bar{\psi}$ were computed separately and then accumulated for 12-hour periods.

1. Forecasts using equation (13) were carried to 48 hours for 4 cases with results which were similar with respect to the features of interest here. In these four cases the contribution of the third term of (13) was isolated. The forecast with initial time 1500 GMT, April 3, 1958, may be taken as representative of this group, and is reproduced as figure 1. During the first 12 hours the vertical advection of vorticity contributed a negative height change[2] everywhere with maximum values of −600 feet. During the second 12-hour period an area of positive changes up to 160 feet appeared, but decreased negative changes persisted over most of the map. During the third 12-hour period some small negative changes persisted, but the positive contributions greatly enlarged with maximum values up to 370 feet. During the last 12-hour period the contributions were everywhere positive with maximum values of 400 feet. The contribution of this term appeared to be mainly large-scale with little detail on the scale of the principal synoptic features.

The phase relationships between h and $\bar{\psi}$ and between h and w are illustrated in figure 2. The vertical velocity field, initially as well as throughout the 48-hour forecast period, was well ahead of the streamline field (upward motion ahead of a trough). On the other hand, the thickness field started out lagging behind the stream function, caught up at around 24 hours, and was well ahead at 48

[2] The quantity ψ occurring in the figures has the dimension length and is derived from $\bar{\psi}$ through the relation $\bar{\psi}=\frac{g}{f_o}\psi$ where g is the acceleration of gravity and f_o is the Coriolis parameter at 45° latitude. In the captions to the figures, ψ is alternatively referred to as height and stream function.

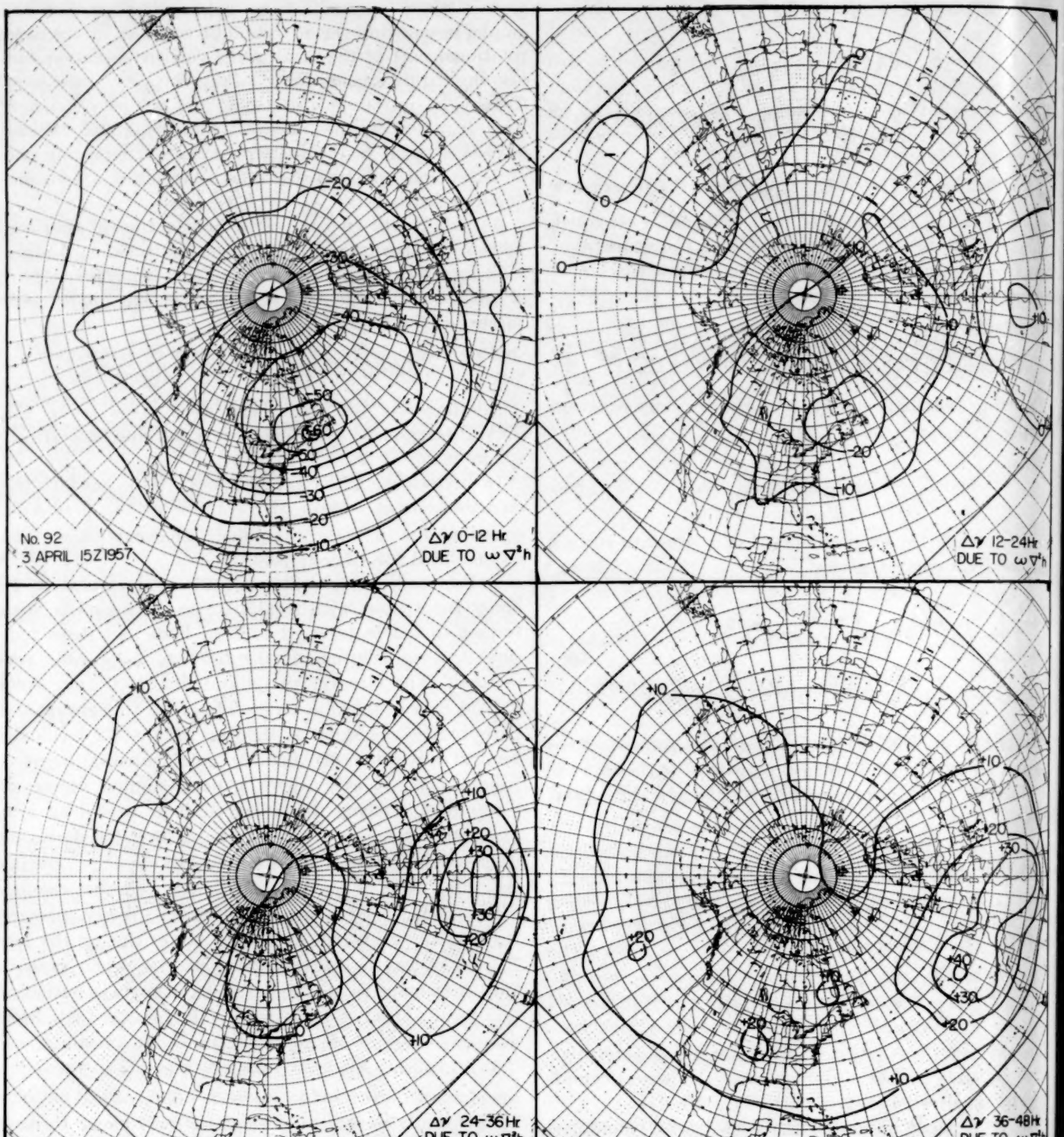

FIGURE 1.—Change in 500-mb. height due to vertical advection of vorticity, labeled in tens of feet.

hours. The error maps show that the stream function field was moved too slowly, and indicate too fast a movement of the thickness field. The w-field versus h-field shows that w and h were positively correlated initially and negatively correlated after 24 hours. This would seem to explain the reversal in the vertical advection of vorticity as time increased.

2. A forecast using (14) was carried to 48 hours, again using as initial data 1500 GMT, April 3, 1958.

In this forecast the thickness field kept its lag better than with the previous model, but during the 36–48-hour period it caught up with the stream function field in

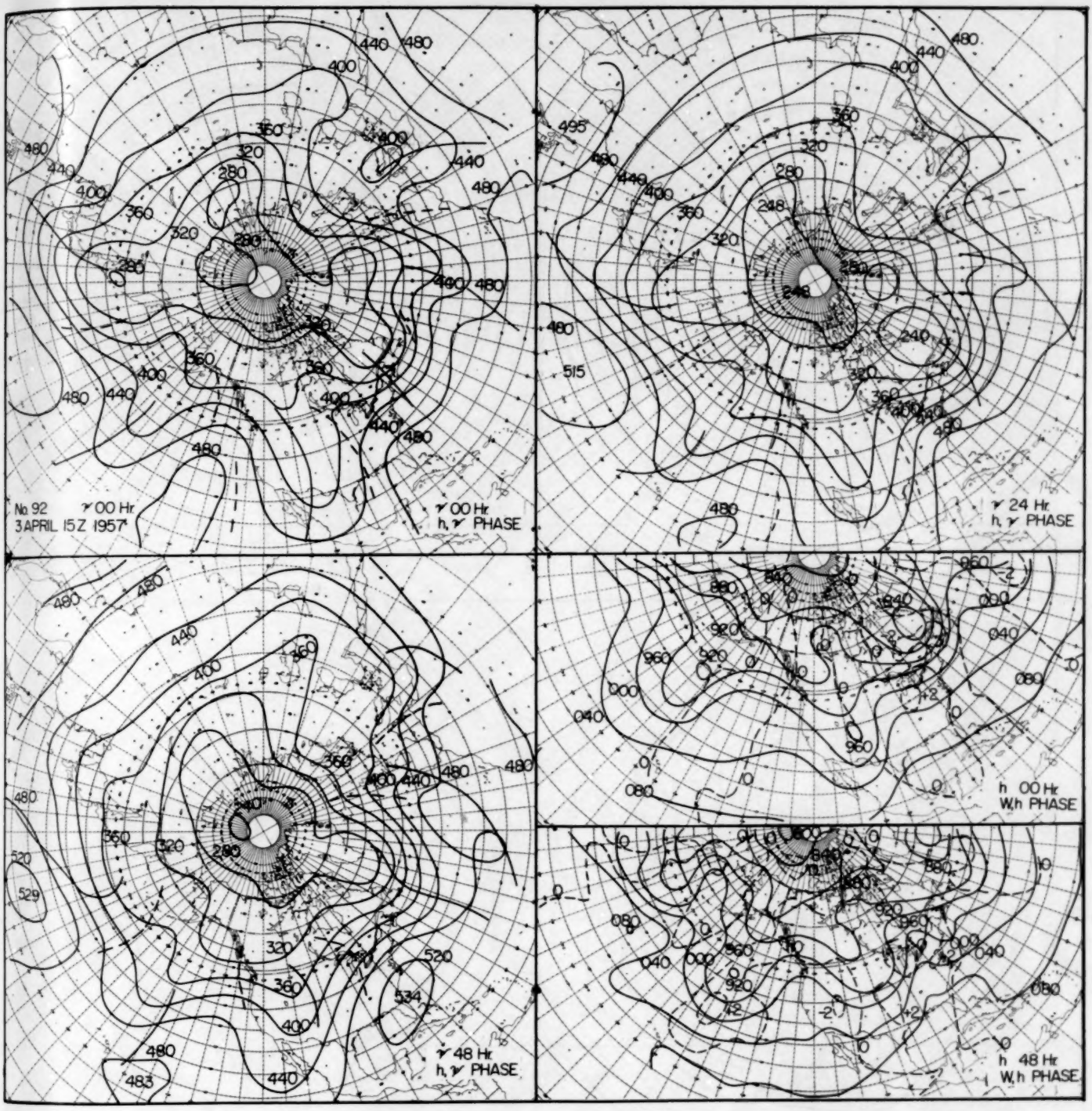

FIGURE 2.—Phase lags between thickness and stream function and thickness and vertical velocity. In portraying the h, ψ phase, dashed lines indicate ridges and short solid lines troughs in the h-field (not contoured); the labeled solid lines are ψ-contours. In the two maps showing the phase between thickness and vertical velocity (h,w), solid lines are thickness contours (in tens of feet) and dashed lines contours for vertical velocity in cm. sec.$^{-1}$.

parts of the map. The vertical advection contribution is shown in figure 3. There was no reversal in the contribution of the vertical advection of vorticity term, but the negative contribution to stream function change was less during the 24–48-hour periods than during the first 24 hours. Vertical velocity had much the same phase relationship to stream function as before, but there is considerable difference in detail between the fields. The 24-hour vertical velocity with (14) was more intense, and the 48-hour vertical velocity slightly more intense than results from using (13).

3. Six forecasts were carried out using equation (15) as one of the basic prognostic equations. Here again the results were similar with respect to the features under

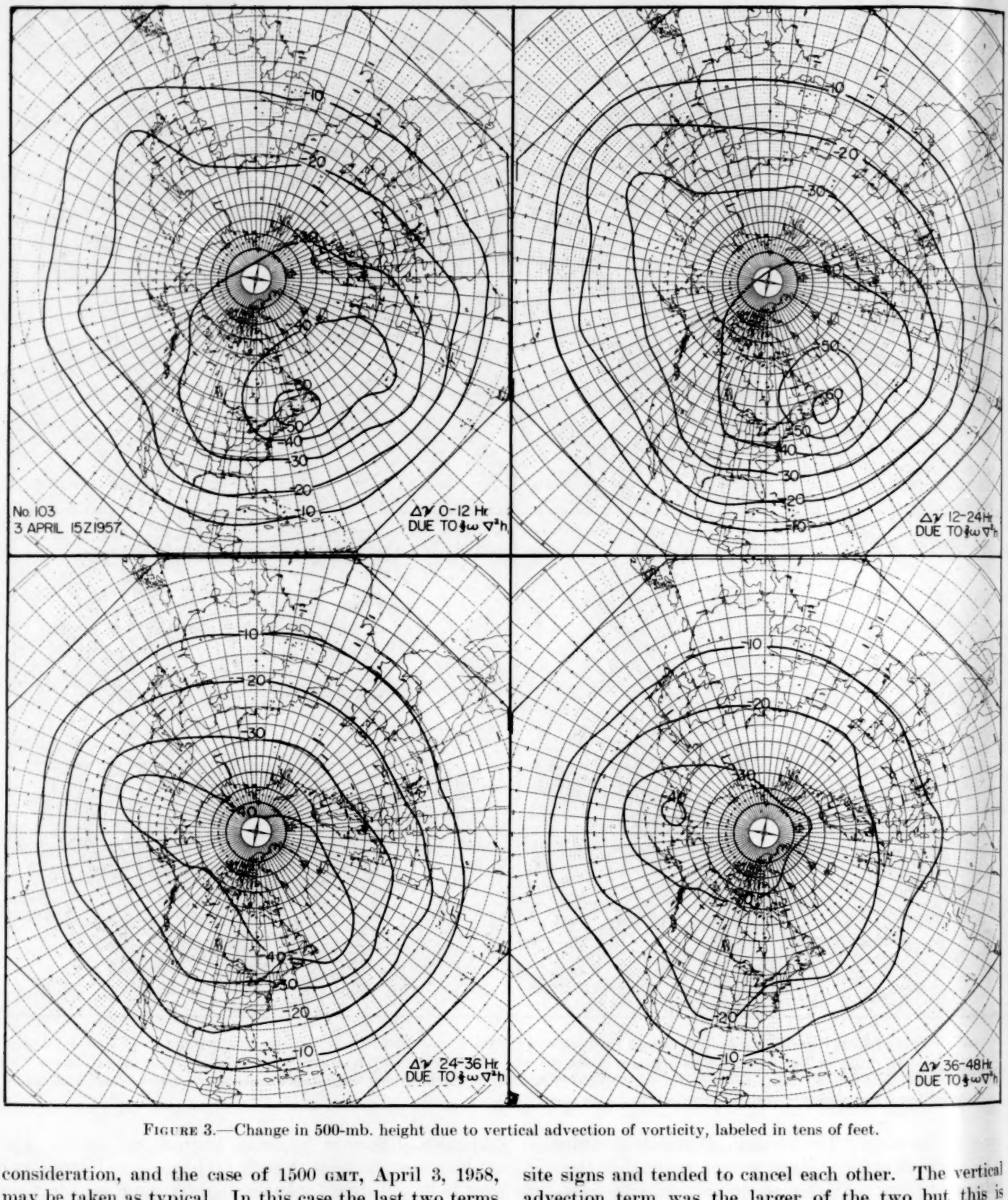

FIGURE 3.—Change in 500-mb. height due to vertical advection of vorticity, labeled in tens of feet.

consideration, and the case of 1500 GMT, April 3, 1958, may be taken as typical. In this case the last two terms of equation (15) were accumulated separately for each 12 hours, the results being given in figure 4. It is seen that the integrated values almost everywhere have opposite signs and tended to cancel each other. The vertical advection term was the larger of the two but this is mainly because of different degrees of truncation. In the vertical advection term, the Laplacian of thickness is formed using the mesh length of d, whereas both of the

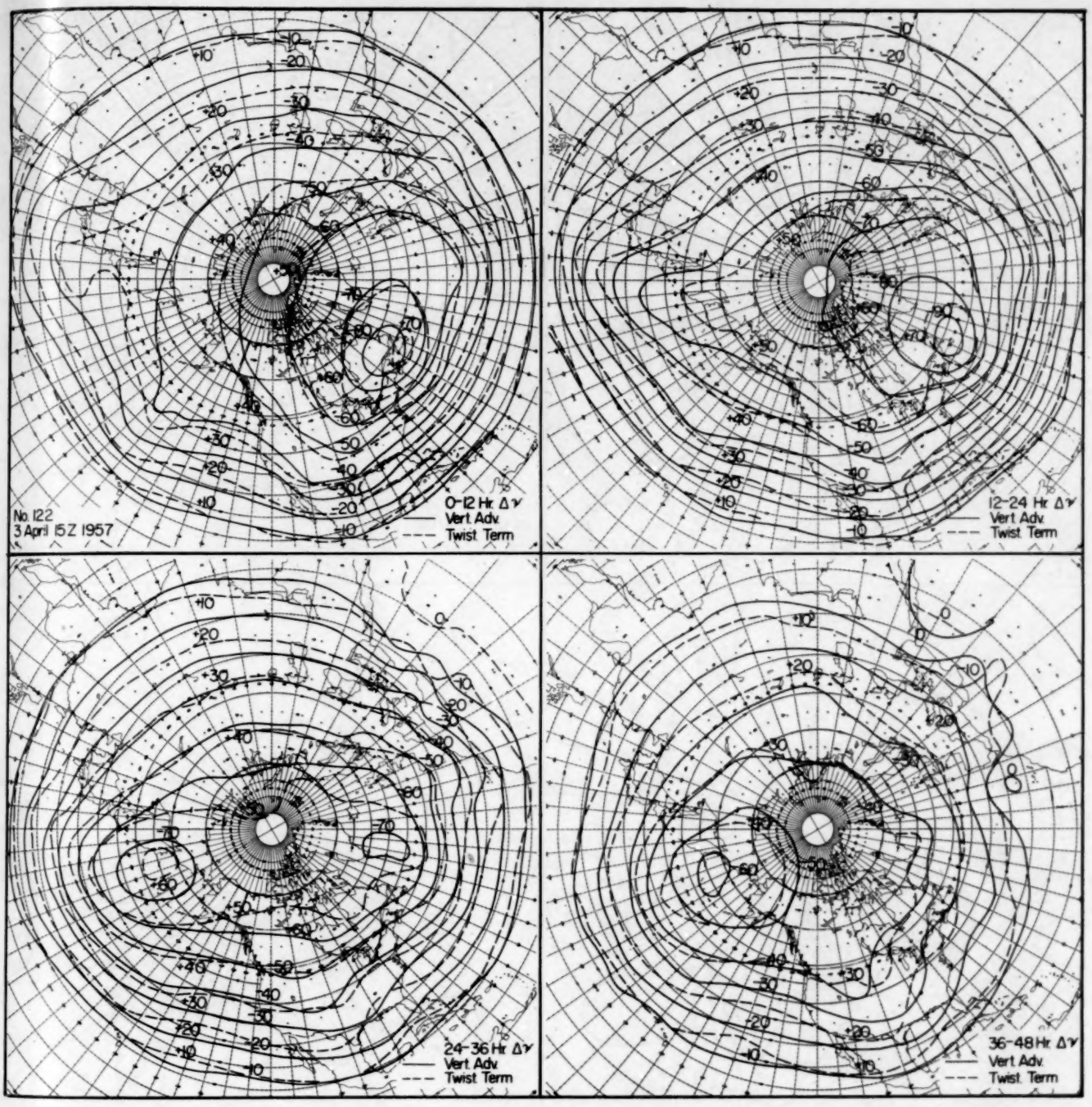

FIGURE 4.—Change in 500-mb. height due to vertical advection (solid lines) and twisting (dashed lines) terms.

first derivatives in the twisting terms have $2d$ as mesh length. When the inconsistency of truncation is removed by combining the two terms it becomes clear, as pointed out earlier, that the net contribution over the grid of the two terms depends only on conditions at the lateral boundaries.

When the last two terms of (15) are combined before finite differences are taken, the accumulated sums take on the values given in figure 5. These may be compared with the results shown in figure 6, which is the sum of the twisting and vertical advection terms of figure 4. These results should be the same except for truncation errors. It thus appears that on a large grid inconsistent truncation of small but systematic terms may alone account for significant forecast error.

It is also to be remarked that in this model and information grid the vertical velocity terms contributed very little in comparison with the error remaining. However, it would be unwise to conclude from this experiment alone that the terms are really unimportant either to the atmosphere or to more sophisticated models.

This model, when corrected for the systematic error

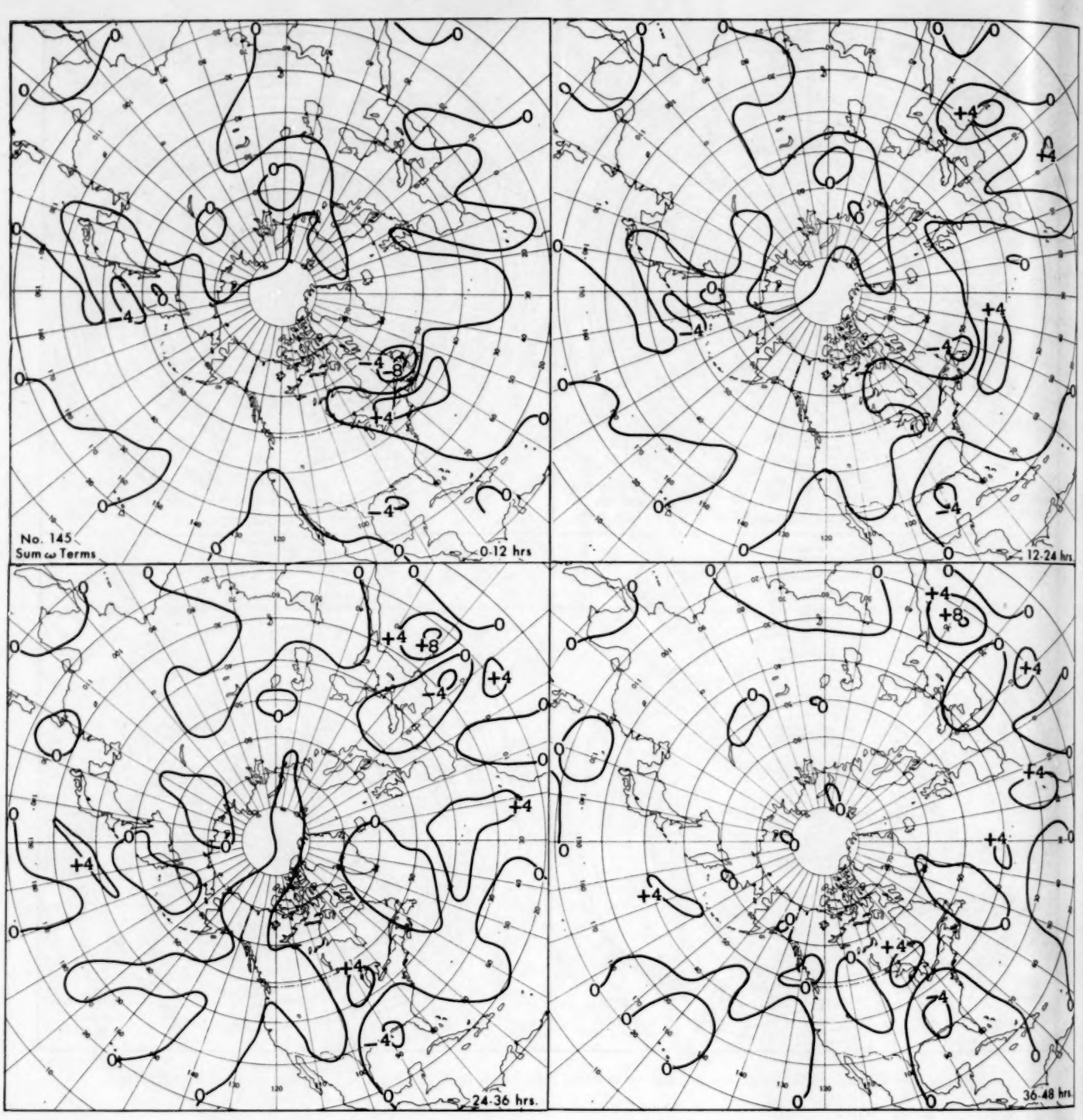

FIGURE 5.—Change in 500-mb. height due to combined vertical advection and twisting terms consistently truncated.

described above, showed a tendency to move the subtropical Highs erroneously westward, and a tendency toward overdevelopment of Lows. The spurious westward movement is presumably a manifestation of this model's incapability of properly forecasting the long waves as discussed by Wolff [2] and Cressman [3]. The overdevelopment is attributed to the third term in equations (14) and (15). This term would seem to be incapable of properly accounting for observed genesis of mean vorticity $\bar{\zeta}$.

5. CONCLUSIONS

The conclusions reached in this study may be summarized as follows:

1. Each of the vertical advection and twisting terms in the vorticity equation tends to have a uniform sign over the entire grid. In a closed system their net contribution is, however, zero when taken together. Omitting one and retaining the other of these two terms leads to spurious creation or destruction of vorticity, devastating to a hemispheric forecast.

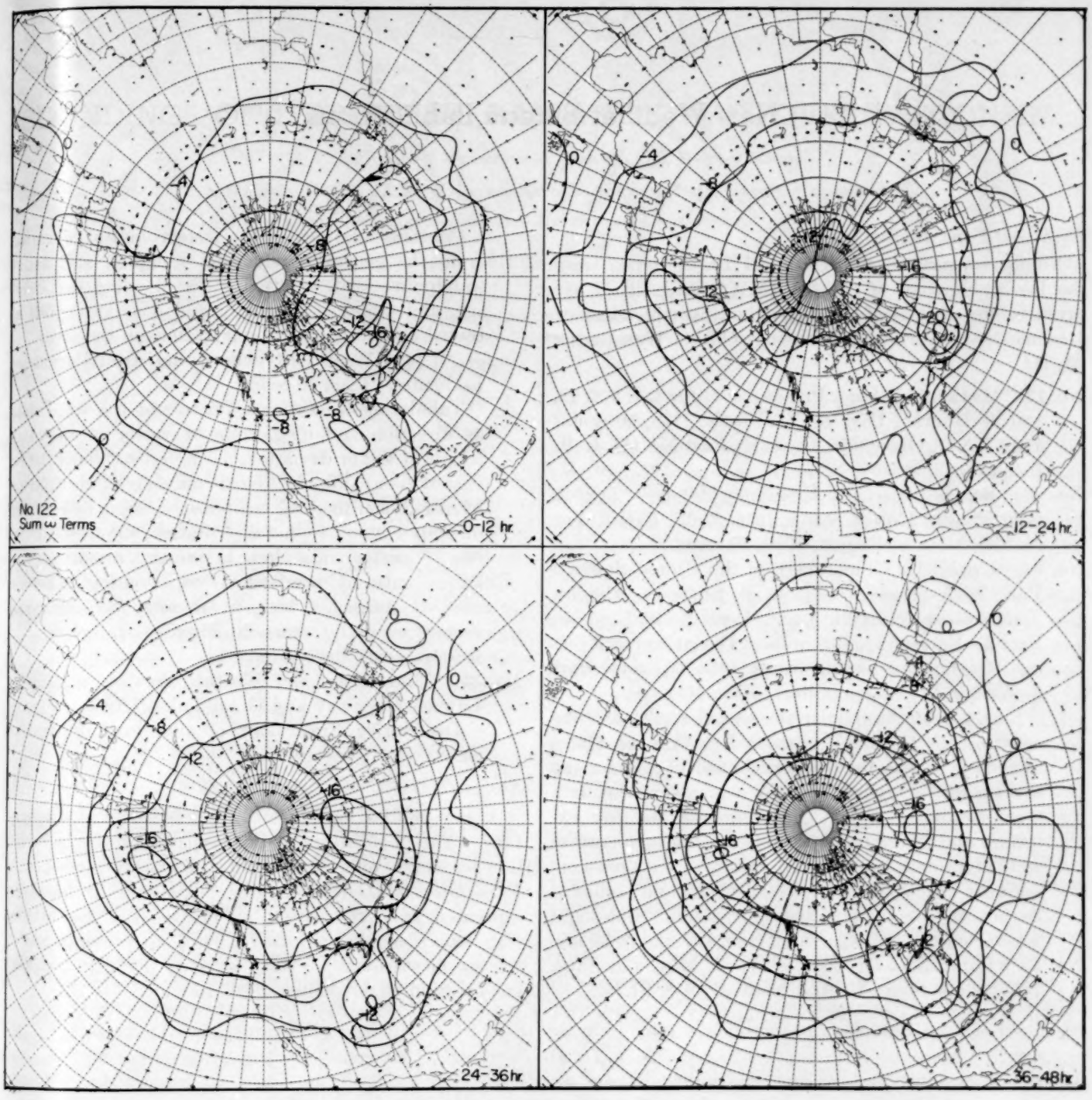

FIGURE 6.—Change in 500-mb. height due to vertical advection and twisting terms inconsistently truncated.

2. When both terms are included, inconsistent truncation may lead to considerable error in the forecast.

3. In approximating the divergence term in the vorticity equation, precaution should be taken not to introduce a small but systematic error of the type referred to under conclusion 1.

4. The contribution of the vertical advection and twisting terms when taken together was insignificant in this model in the six cases tested.

508099—59——2

REFERENCES

1. P. D. Thompson, "A Two-Level Model with Effects of Vertical Velocity Advection, Irregular Terrain, and Variable Static Stability," Office Note No. 6, Joint Numerical Weather Prediction Unit, June 1957.
2. P. M. Wolff, "The Error in Numerical Forecasts Due to Retrogression of Ultra-Long Waves," *Monthly Weather Review*, vol. 86, No. 7, July 1958, pp. 245–250.
3. George P. Cressman, "Barotropic Divergence and Very Long Atmospheric Waves," *Monthly Weather Review*, vol. 86, No. 8, August 1958, pp. 293–297.

New Weather Bureau Publications

Technical Paper Series

Numbers issued in the Technical Paper Series since the last publication of the list (MWR Aug. 1957) are given below. All are for sale by the Superintendent of Documents, Government Printing Office, Washington 25, D.C.

No. 15. "Maximum Station Precipitation for 1, 2, 3, 6, 12, and 24 Hours": Part XXI, Illinois, 1958, 50 cents; Part XXII, Ohio, 1958, 65 cents; Part XXIII, California, 1959, $1.50.

No. 29. "Rainfall Intensity-Frequency Regime": Part 2, Southeastern United States, 1958, $1.25; Part 3, The Middle Atlantic Region, 1958, 30 cents.

No. 32. "Upper-Air Climatology of the United States": Part 1—Averages for Isobaric Surfaces, Height, Temperature, Humidity, and Density, 1957, $1.25; Part 2—Extremes and Standard Deviations of Average Heights and Temperatures, 1958, 65 cents; Part 3—Vector Winds and Shear, 1959, 50 cents.

Part 1 contains tabulations and charts by months covering the Caribbean area and the United States including Alaska for the period 1946–55 and for the surface to the highest level for which sufficient data were available. Part 2 contains the monthly extremes and standard deviations for the temperature and height data presented in part 1. Part 3 presents seasonal charts of mean vector winds and standard deviations covering only the contiguous 48 States and for various pressure surfaces from 700 mb. to 30 mb.

No. 33. "Rainfall and Floods of April, May, and June, 1957 in the South-Central States," 1958, $1.75.

Contains analyses of the meteorological situation from the general circulation, synoptic, and radar standpoints, a description of the flooding and damage, and tables of the daily and hourly rainfall at recording and nonrecording stations in the area.

No. 34. "Upper Wind Distribution Statistical Parameter Estimates," 1958, 40 cents.

Tabulations of such parameters of the wind data as direction and magnitude of vector mean wind, standard vector deviation, mean and standard deviation of zonal and meridional components, correlation of meridional to zonal components, angle of rotation of elliptic axes of wind distribution, standard deviation of components along major and minor axes of ellipse, ratio of standard vector deviation to square root of difference between squares of scalar and vector means. Covers Northern Hemisphere and mostly period 1948 to 1953.

No. 35. "Climatology and Weather Services of the St. Lawrence Seaway and Great Lakes," 1959, 45 cents.

Descriptive climatology of area with illustrative charts.

Storm Data

A new publication *Storm Data* was begun in January 1959. This monthly periodical consists of the information on storms and storm damage formerly contained in *Climatological Data—National Summary*. It has been separated from the parent publication and the tabulation somewhat streamlined to speed up presentation of the storm statistics. Price: 15 cents per copy; annual subscription $1.50 domestic, $2 foreign.

SOUNDINGS OF TERRESTRIAL RADIATION FLUX OVER WISCONSIN[1]

P. M. KUHN, Office of Meteorological Research, U.S. Weather Bureau

V. E. SUOMI and G. L. DARKOW, Department of Meteorology, The University of Wisconsin

[Manuscript received January 6, 1959; revised April 7, 1959]

ABSTRACT

Results and conclusions drawn from 50 radiometer-sonde ascents over Wisconsin are presented. Atmospheric infrared radiation flux is separated into upward, downward, and net components. Radiation divergence and resulting cooling are computed. Seasonal averages of these direct observations are compared.

1. INTRODUCTION

In the past, direct measurements of the atmosphere's radiative balance have been costly and complex. Suomi, Staley, and Kuhn [1] recently reported on a radiometer-sonde which was designed as a routine technique for obtaining vertical profiles of the flux of infrared radiation in the atmosphere. This instrument has been successfully adapted to balloon-borne flights, and briefly, consists of the economical net radiometer described by Suomi and Kuhn [2] attached to the standard U.S. Weather Bureau radiosonde. An electrically driven sequencer and simple circuit modifications are necessary.

SYMBOLS USED IN TEXT

$\partial T/\partial t$	Change in temperature in °C. per day.
g	Acceleration due to gravity, c.g.s. units.
R_{NU}	Net radiation in langleys per minute at top of layer ($R_{NU}>0$ directed upward).
R_{NL}	Net radiation in langleys per minute at bottom of layer ($R_{NL}>0$ directed upward).
c_p	Specific heat of air, c.g.s. units.
Δp	Thickness of layer in millibars.
σ	Stefan-Boltzmann constant, c.g.s. units.
T_b	Observed temperature of bottom sensor.
T_t	Observed temperature of top sensor.
C_i	Internal conduction for radiometer in langleys per minute.
C_t	Top conduction for radiometer in langleys per minute.
C_b	Bottom conduction for radiometer in langleys per minute.
E_b	Error term for bottom half of radiometer, langleys per minute.
E_t	Error term for top half of radiometer, langleys per minute.

NOTE.—Values of radiation flux or net radiation >0 indicate a flux or net flux directed away from the air-ground interface.

[1]The research reported in this study is supported by the Office of Meteorological Research, U.S. Weather Bureau.

2. TYPICAL RADIOMETER FLIGHTS

The radiometer-sonde flights were carried out at the University of Wisconsin at Madison, Wis. The flight program included (i) direct measurement of the upward, downward, net, and total components of infrared radiation flux; and (ii) computation of radiative cooling of the atmosphere.

Figures 1 through 3 show three typical nocturnal ascents. In each, the upward, $R\uparrow$, downward, $R\downarrow$, and net, R_N, radiation currents in langleys per minute are shown, together with the air and dewpoint temperatures. The radiative temperature change of the air column is calculated from the vertical divergence of radiation in 50-mb. layers up to the 200-mb. level and for 25-mb. layers above that from the expression,

$$\frac{\partial T}{\partial t}=\frac{-g(R_{NU}-R_{NL})}{c_p\Delta p} \tag{1}$$

This profile, given in degrees Celsius change per day, appears on the right for each figure.

Figure 1 is a clear summer night sounding and illustrates characteristic features of many similar flights. In all such cases relative warming occurs just beneath any inversion, including the tropopause. In particular, the warming was evident at 815 mb. during the flight of July 7, 1958, beneath a low-level inversion. Again at 270 mb., warming occurred beneath the tropopause inversion. The latter phenomenon is clearly visible immediately below the tropopause in the summer mean cooling profile. Frequently, such radiative warming becomes positive, at times reaching from 2° to 3° Celsius heating per day. For example, a warming of 1.0° C. per day occurred at 270 mb. on the July 7, 1958, ascent.

Secondly, in many instances we find the strongest cooling just above inversions or cloud layers. In detail, this may be seen in figure 1 at 680 and 165 mb., reaching over 2.0° C. in each case. Figure 1 might be compared with the observed cooling rate obtained by Brewer and Houghton [3] for July 20 and 21, 1956.

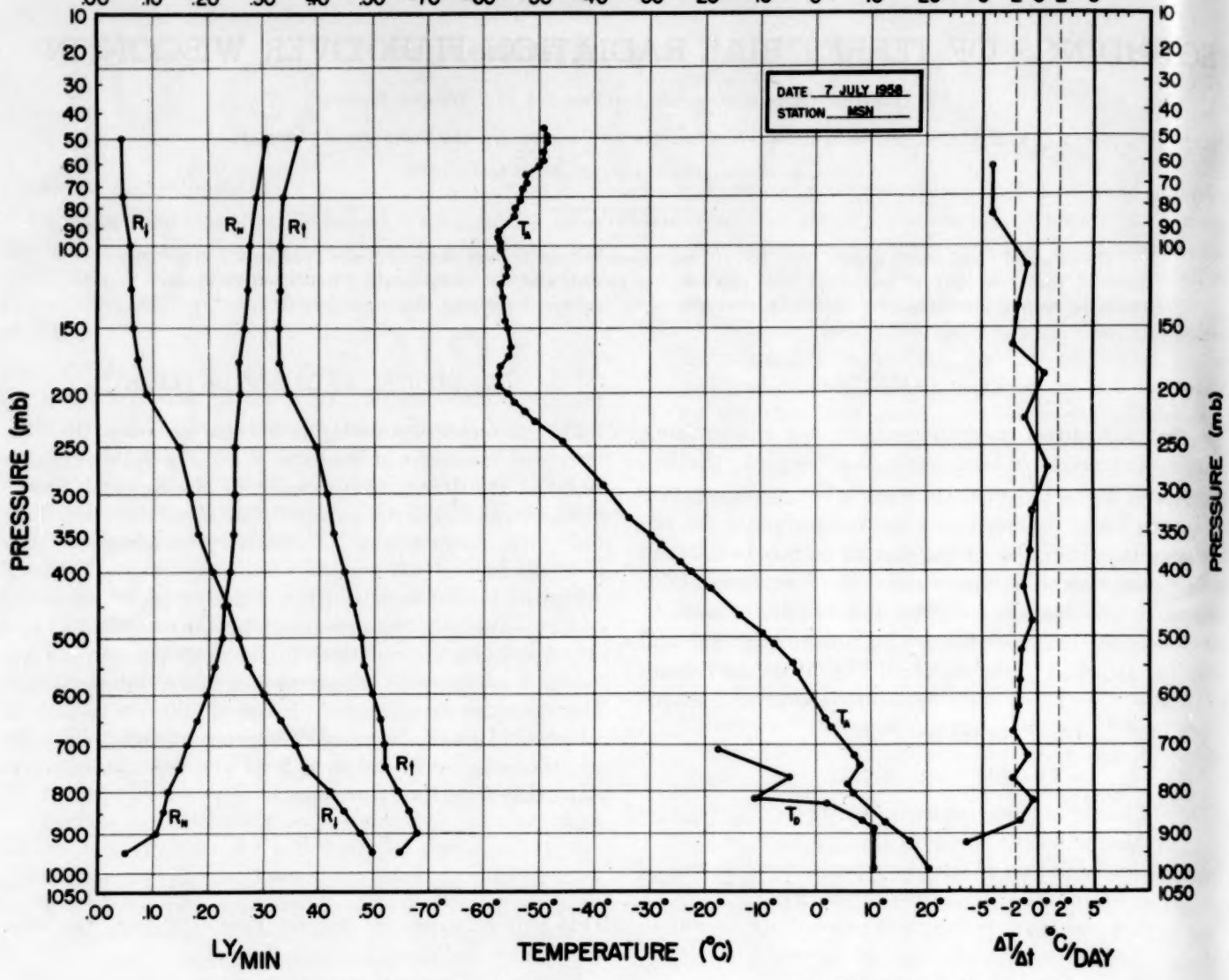

FIGURE 1.—Clear summer radiometer-sonde ascent. July 7, 1958, 2000 CST, Madison, Wis.

The clear nocturnal winter sounding, figure 2, provides a typical cooling profile often observed in the winter. The average cooling of this winter profile, except for the microlayer, is 1.0° C. per day, as compared with a summer average cooling rate of 1.7° C. per day. Thus direct radiation measurements allow a computation of radiative cooling far above the limits of chart evaluation. Between 250 and 200 mb., there is indication of the ascent passing above effective atmospheric radiators. Both the upward and downward radiation currents approach a constant value even though there is a positive gradient in the temperature profile. The last plotted point in the upward stream is doubtful.

A cloudy winter ascent, figure 3, demonstrates the radiative effects of cloud. Below the stratocumulus base at 870 mb. there is radiative warming. At the cloud top, however, there is a sharp gradient in the downward directed radiation, $R\downarrow$, resulting in strong radiative divergence and a cooling rate of 8.5° C. per day. The break into the clear night sky at 725 mb. sharply reduces the downward propagating current. The gradient of $R\downarrow$ increases from −0.03 ly./min. per 50 mb. to −0.09 ly./min. per 50 mb. In the layer between 100 and 150 mb., regardless of slowly falling air temperatures, the upward and downward radiation currents become essentially constant. This further indicates a decrease in atmospheric radiators.

3. AVERAGE SOUNDINGS

CLEAR WINTER

An average cooling rate for clear winter ascents was obtained by averaging the upward, downward, and net components of the radiative flux in 50-mb. steps for 12

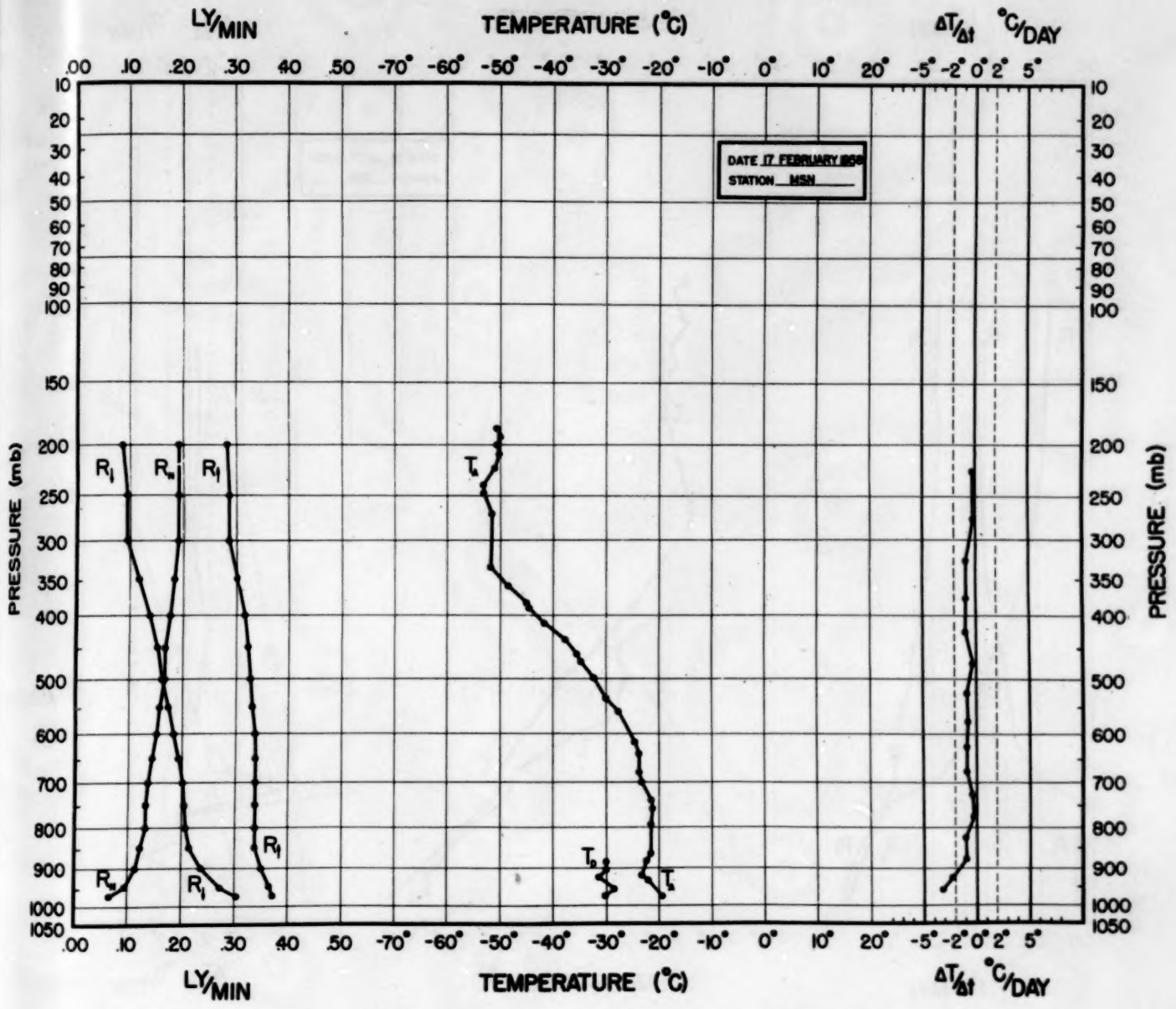

FIGURE 2.—Clear winter radiometer-sonde ascent. February 17, 1958, 2136 CST, Madison, Wis.

ascents. Cooling was then computed from these results providing a mean vertical distribution of the terrestrial radiation and its divergence. A simple computation, equation (1), gives the profile of cooling. In figure 4 this average cooling is compared with Möller's [4] indirect estimate of the mean mid-latitude annual infrared cooling. Except for the observed decrease in cooling just beneath the mean height of the tropopause, the indirect estimates coincide favorably with the directly measured cooling. London's [5] computation of the mean March infrared cooling also lies well within a comparable range but is offset in season. Between 150 and 200 mb. there is a tendency for constancy in $R\downarrow$ and $R\uparrow$, though it is not as evident as in the average summer profiles.

CLEAR SUMMER

The 12 summer flights, reaching a mean height of 75 mb., furnish a representative mid-latitude average of the vertical distribution of radiative fluxes and the infrared atmospheric cooling for a continental climate. The data of figure 5 are presented in the manner of figure 4.

Between 70 and 150 mb. in the average summer soundings, the gradient of the downward- and upward-directed radiation fluxes tends to zero. This indicates that under clear summer conditions there exists a marked decrease in atmospheric radiators near the 100-mb. level and above. The mean cooling averages 1.7° C. per day compared with a mean winter cooling of 1.0° C. per day.

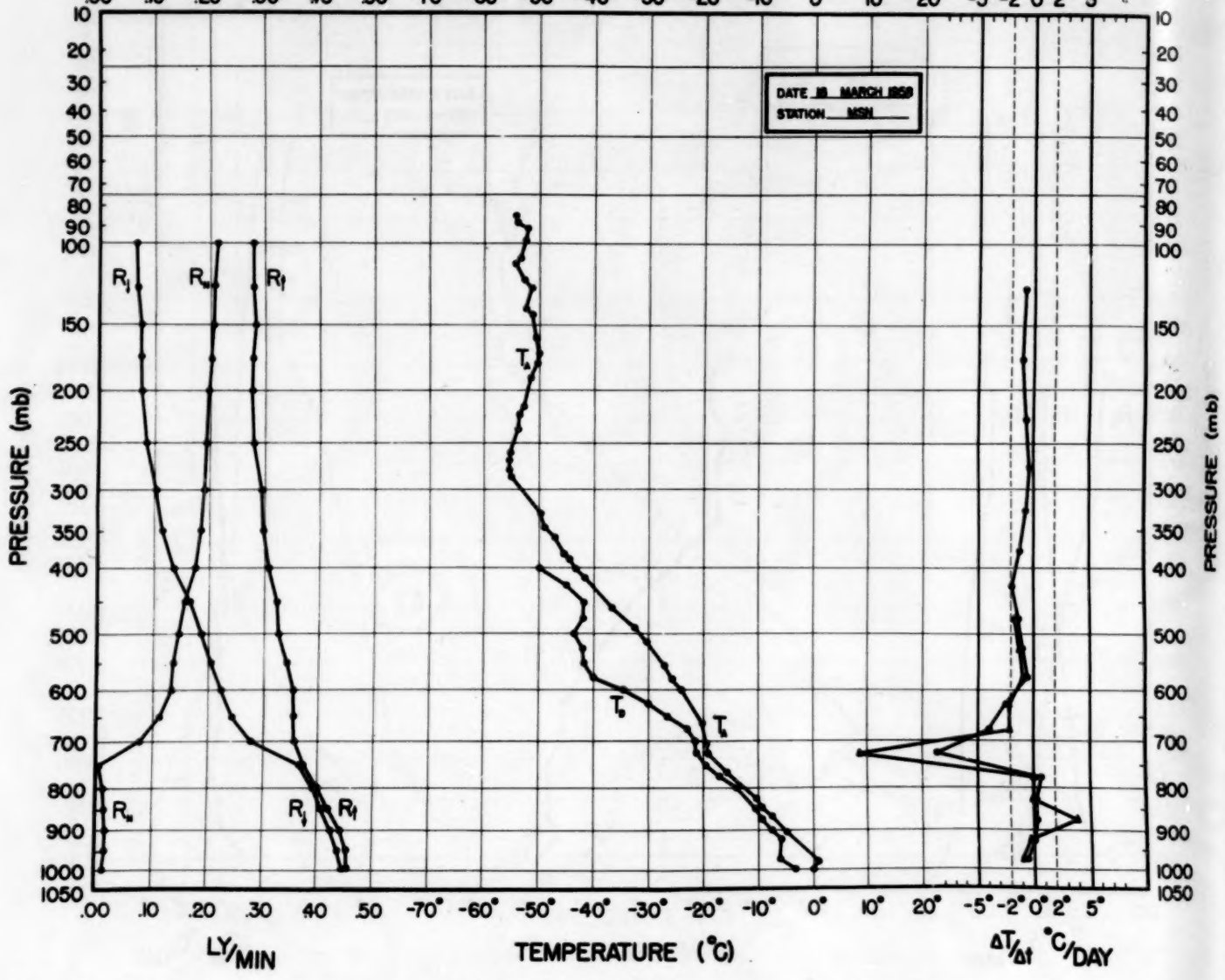

FIGURE 3.—Cloudy winter radiometer-sonde ascent. March 18, 1958, 2033 CST, Madison, Wis. Triangles represent Elsasser cooling evaluation. Circles indicate direct evaluation of radiative cooling.

4. TERRESTRIAL RADIATION

The values of this outgoing terrestrial (net) radiation for only the highest flights, clear and cloudy, in which the observed vertical gradient of the net radiation becomes zero, are averaged in table 1. For comparison, the estimates of Robinson [6] at Kew, Lettau [7] for Northern Hemisphere annual average, and Houghton [8] for Northern Hemisphere annual average are included.

TABLE 1.—*Outgoing terrestrial (net) radiation, langleys per minute*

Summer		Annual		Winter	
Madison Average	0.310	Lettau	0.320	Madison Average	0.220
Robinson (Kew)	.320	Houghton	.320	Robinson (Kew)	.270
		Madison	.265		

5. CLOUD EFFECTS

A characteristic phenomenon associated with ascents through clouds appears in figure 3 at 725 mb. Very strong radiative divergence immediately above a cloud top appears as an excellent indicator of the cloud top. This feature is obviously caused by the rapid decrease in the downward current of radiation measured by the upward-facing surface of the radiometer as it breaks into the clear night sky above the clouds.

6. ELSASSER CHART COMPARISON

The cooling profile indicated by triangular points in figure 3 represents an Elsasser evaluation for this flight.

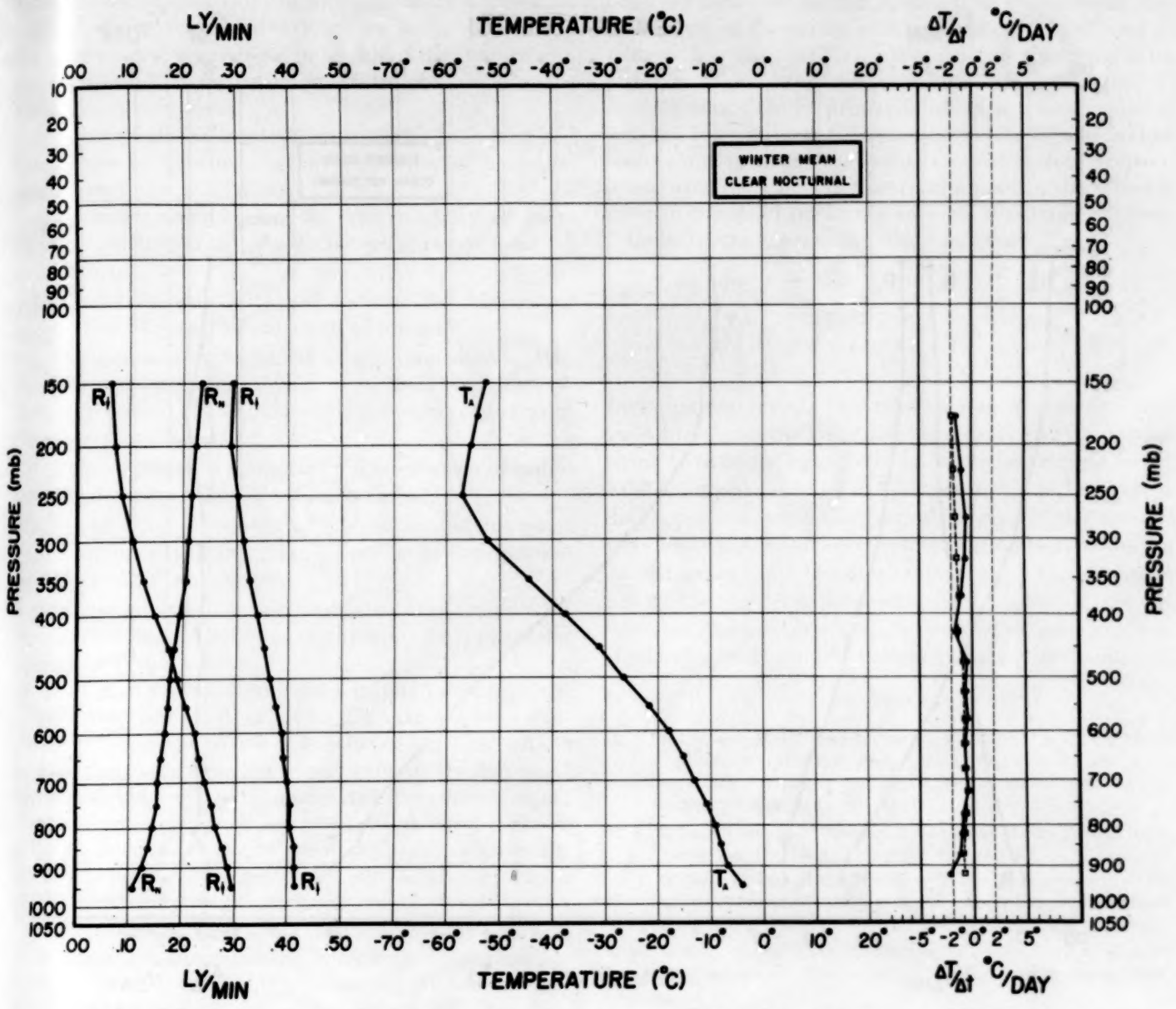

FIGURE 4.—Winter mean clear nocturnal ascent. Squares indicate annual cooling rate estimate by Möller.

Omitting that portion of the Elsasser [9] computation which is dependent upon assumptions made for the cloud emissivity, we find the general agreement between the direct and indirect cooling evaluation good. However, the humidity element was out of range above 450 mb., eliminating an Elsasser evaluation for nearly two-thirds of the ascent. On the basis of the indirect chart radiation evaluations for a limited number of flights, the radiation values appear somewhat underestimated when compared with our direct measurements. This will be the subject of a forthcoming report. The magnitude of the directly measured warming and cooling below and above cloud bases and tops agrees with indirect estimates of Möller [4].

7. PRACTICAL APPLICATIONS

Some of the apparent practical applications of the radiometer-sonde ascents are for cloud top determinations and in studies of cloud dissipation, propagation to the surface of high-level heating and cooling, stability changes, and the role of long-wave radiational destabilization as a trigger mechanism for nocturnal thunderstorms. The actual measurement of the infrared components under a variety of situations is providing a valuable tool with which these applications can be studied.

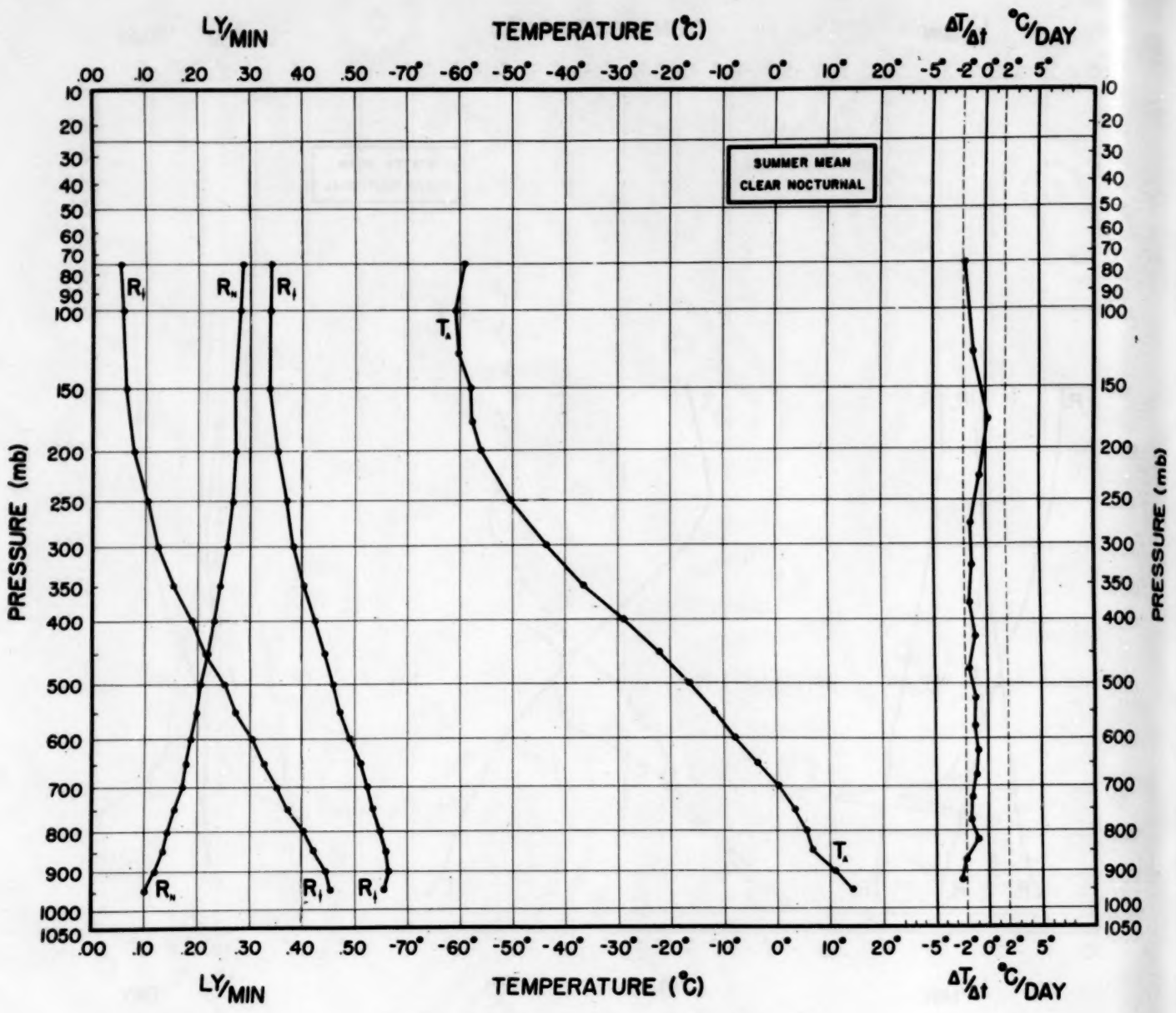

FIGURE 5.—Summer mean clear nocturnal ascent.

8. SATELLITE METEOROLOGY IMPLICATIONS

There is, of course, a natural tie between satellite radiation measurements and similar measurements with the radiometer-sonde. One might state that the balloon-borne radiometer fills in details integrated out by satellite measurements. Primarily, a radiometer-sonde network could augment the satellite measurements. Of necessity the satellite horizontally integrates radiation measurements of the earth and atmosphere over large areas because of its great speed and height. On the other hand, radiometer-sonde observations, though limited in height, provide exceptional vertical detail over a limited area. The satellite measures the large-scale radiation balance of the earth-atmosphere system from a point in space. The radiometer-sonde measures radiative fluxes within the earth-atmosphere system.

9. ACCURACY OF MEASUREMENTS

Standard calibration procedure includes a separate base line check at three temperatures of the three thermistors used in each flight, together with a surface check of the actual net radiation against a suitable standard.

Many additional tests and precautions, their actual details too extensive for this report, are either routinely performed in preparation for each flight or have been conducted as controlled experiments. Among these are the following:

1. Dry nitrogen purging of each radiometer prior to flight to prevent internal moisture condensation.

2. Individual calibration of the three thermistor sensors to prevent systematic errors.

3. Use of proportional changes in both vertical and

horizontal dimensions of the radiometer as a check on validity of the conduction terms.

4. Use of discrete changes in length of flight train as a check on solid angle intercept of balloon in affecting radiation measurement.

5. Substitution of bead thermistors for standard rod thermistors to improve lag characteristics of radiation sensing surfaces.

6. Extensive computations of transmissivity of polyethylene ventilation shield cells covering range from 0.8 to 40 microns.

7. Extending emissivity calculations for blackening agent, black "Decoret" Enamel, to 40 microns.

8. Comparison, in flight, of single- and double-layer polyethylene ventilation shields as to their respective effects on the ratio of conduction to convection transfers in these horizontal layers.

9. Tests of effects of nonhorizontal orientation of radiometer in flight by means of pendulum effect.

10. Evaluation of validity of internal conduction term, C_i, in equation (1) through its elimination in a comparison flight of a "disc" radiometer.

11. Determination of the profile of the gradient of temperature in the horizontal through the radiometer through multiple sensors.

The effects of a flight trajectory through clouds on the absolute accuracy of either $R\downarrow$ or $R\uparrow$ have not been completely determined. While it is believed that such effects on radiation measurements as moisture on the top polyethylene shield are rapidly eliminated due to ventilation, this is being carefully investigated. The rapid decrease in the magnitude of the downward propagating radiation current indicates a diminution in this assumed adverse effect immediately upon exit from cloud.

A careful error analysis has been made of the accuracy of temperature measurement including these random errors: thermistor error, thermistor lag, recorder error, calibration error, and transmitter error [10]. The "accuracy" ascribed to any measuring instrument may be misleading because of the many ways of estimating and expressing accuracy. Customarily, we employ various statistical measures of dispersion to indicate this accuracy and those most often used are the standard deviation, the average deviation, and the probable error. Their interrelation is well known. However, we will limit our error discussion to the standard deviation, σ. The root of the sum of squares of individually computed temperature measurement standard deviations in the error analysis mentioned above provides a value for one standard deviation, σ, of 0.4° C. Setting out confidence limits at 95 percent, we must accept a maximum error (2σ) of 0.8° C. Such a random error becomes most important in computing atmospheric cooling and can possibly result in maximum cooling errors of up to ±1.2° C. This maximum cooling rate error is large in comparison to some of the observed mean values, but it should be remembered that 95 percent of the errors will be less than 1.2° C. and 67 percent less than 0.6° C. We are experimenting with methods of reducing this maximum error to ±0.5° C. Such methods center primarily about a measurement of ΔT, the temperature difference between top and bottom sensors, rather than the absolute top and bottom temperatures, which can go far toward eliminating the inherent error in the small difference between two large numbers.

Consider the expression for net radiation, R_N,

$$R_N=\sigma(T_b^4-T_t^4)$$
$$+1.37\left[2C_t+C_t-C_b+\lambda\frac{d}{dt}(T_b-T_t)+E_b-E_t\right] \quad (2)$$

Investigation reveals the relative size of the first and second terms on the right, the black-body and conduction terms, to be in the ratio 1.0 to 0.6 in the lower flight levels. At the tropopause this ratio changes to 1.0 to 1.8. Above the tropopause with the vertical change in the upward and downward radiation currents tending to zero, the lag term, third on right, becomes insignificant. The maximum size of the lag term never exceeds 5 percent of the net radiation and this occurs only in cases of extreme gradient of the observed top and bottom radiating temperatures.

REFERENCES

1. V. E. Suomi, D. O. Staley, and P. M. Kuhn, "A Direct Measurement of Infra-red Radiation Divergence to 160 mb.," *Quarterly Journal of the Royal Meteorological Society*, vol. 84, No. 360, Apr. 1958, pp. 134–141.
2. V. E. Suomi and P. M. Kuhn, "An Economical Net Radiometer," *Tellus*, vol. 10, No. 1, Feb. 1958, pp. 160–163.
3. A. W. Brewer and J. T. Houghton, "Some Measurements of the Flux of Infra-red Radiation in the Atmosphere," *Proceedings of the Royal Society (A)*, vol. 236, Aug. 1956, pp. 175–186.
4. F. Möller, "Long-Wave Radiation," *Compendium of Meteorology*, American Meteorological Society, Boston, Mass., 1951, pp. 34–49.
5. J. London, "The Distribution of Radiational Temperature Change in the Northern Hemisphere during March," *Geophysical Research Papers* No. 18, Geophysics Research Directorate, Air Force Cambridge Research Center, Bedford, Mass., 1952, 64 pp.
6. G. D. Robinson, "The Use of Surface Observations to Estimate the Local Energy Balance of the Atmosphere," *Proceedings of the Royal Society (A)*, vol. 236, Aug. 1956, pp. 160–171.
7. H. Lettau, "A Study of the Mass, Momentum, and Energy Budget of the Atmosphere," *Archiv für Meteorologie, Geophysik, und Bioklimatologie, Ser. A*, vol. 7, 1954, pp. 133–157.
8. H. G. Houghton, "On the Annual Heat Balance of the Northern Hemisphere," *Journal of Meteorology*, vol. 11, No. 1, Feb. 1954, pp. 1–9.
9. W. M. Elsasser, "Heat Transfer by Infrared Radiation in the Atmosphere," *Harvard Meteorological Studies*, No. 6, Harvard University, 1942, 107 pp.
10. Air Weather Service, "Accuracies of Radiosonde Data," *Air Weather Service Technical Report* 105–133, Washington, D.C., Sept. 1955.

508099—59——3

THE DISTRIBUTIONS OF FREEZE-DATE AND FREEZE-FREE PERIOD FOR CLIMATOLOGICAL SERIES WITH FREEZELESS YEARS*

H. C. S. THOM

Office of Climatology, U.S. Weather Bureau, Washington, D.C.

[Manuscript received December 3, 1958; revised March 4, 1959]

ABSTRACT

It is shown that the freeze distribution is a mixture of the distribution of freeze-date and the simple dichotomous distribution of freeze and freezeless years. This is applied both nonparametrically and assuming a normal distribution of freeze date to three stations at three different thresholds to obtain the probabilities of freeze before or after any date. The distribution of the freeze-free period is developed and application made to one of the stations to obtain probabilities of the freeze-free period being less than a given time interval. The expressions for the mean freeze-date and freeze-free period are also developed and estimates made for the stations treated.

1. INTRODUCTION

The estimation of freeze probabilities from complete freeze-date series has been treated by Thom and Shaw [1]. When the freeze-date series for an observation station is *incomplete* in the sense that some years experienced no freeze, there is, of course, a probability of freezeless years. This is common in more southerly latitudes, especially for freeze thresholds below 32° F. With the addition of the no-freeze probability component, a quite different problem in the estimation of freeze probability arises. This has been discussed by Spillman et al. [2]. They gave rules for finding the mean recurrence interval for the incomplete series; but since they did not recognize the more general statistical aspects of the problem, their rules are not completely convertible to probability statements.

2. THE FREEZE DISTRIBUTION FUNCTION

The model for determining freeze probability may be thought of as a mixture of two distributions: one a discrete distribution of no-freeze and freeze, the other an essentially continuous distribution of freeze-date for years when freeze occurred. In this discussion, the period over which spring freeze-date is assumed to range is January 1 to June 30, and that for fall freeze is from July 1 to December 31. These are arbitrary, and other dates may be assumed if it suits a particular purpose better, as we shall see later. The model is seen to be equivalent to concentrating a probability of no-freeze at an arbitrary point before the beginning of the season for spring freeze and after the season for fall freeze.

We define the spring freeze-date series as in [1] to be the series of annual last dates in spring on which a minimum temperature less than the threshold temperature (32°, 28°, 24°, 20°, 16°) has occurred. The fall freeze-date series is defined by substituting the words *fall* for spring and *first date* for last date.

On the basis of the results given in [1], we shall assume that the climatological series comprising freeze-dates mixed with no-freeze occurrences are random variables. It follows then that the distribution functions of freeze may be found, and that these will completely define the freeze series populations.

The distribution function is defined as usual by

$$F(x)=\int_{-\infty}^{x} f(u)\,du \tag{1}$$

where $f(u)$ is the probability density function (pdf) or frequency distribution and $F(-\infty)=0$ and $F(\infty)=1$. Here $F(x)$ is the probability that u is less than x; and when u is continuous this is identical with the probability of a value less than or equal to x. Clearly in the spring we shall be most interested in the probability of a freeze occurring after x, and hence, we shall be interested in the form $1-F(x)$ which gives that probability. In fall we shall be interested in the probability of a freeze before x which is given by $F(x)$ itself.

The mixed distribution of freeze-date and no-freeze for spring may now be derived as follows: Let q_s be the probability of no-freeze occurring in spring according to the model assumed above. $1-q_s=p_s$ is then the probability of a freeze after the beginning of the freeze season. According to the definition of mixed distributions [4], the distribution function for spring freeze will be

$$G(x)=q_s+p_s F_S(x) \tag{2}$$

where $F_S(x)$ is the distribution function of spring-freeze date when freeze occurred. We employ large S and A to indicate the continuous portion of x, and small a and b to indicate the discrete portion. It is seen that $G(x)$ is

*This paper is based on work done while the writer was Visiting Professor of Statistics, Biometrics Unit, Cornell University [3].

a distribution function, for if x takes a small value b by definition $F(b)\sim 0$, meaning that no freeze-date will occur before b where $G(b)=q_s$. This is the probability that no-freeze will occur. If x is not a member of either s or S, then $G(x)=0$, for it is impossible that either one of the events freeze or no-freeze should occur. On the other hand, if x is a large value, c, then by definition $F(c)\sim 1$, and $G(x)=q_s+p_s=1$ which is the probability that either no-freeze or a freeze-date have occurred before c. Thus (2) is a distribution function. It will be clear now that the probability of a freeze after date x will depend not only on $1-F(x)$, the probability of freeze-date when freeze has occurred, but also on the probability that a freeze will occur at all on any date. This, of course, is $1-q_s$ or p_s.

As we have seen, $G(x)$ of equation (2) gives the probability of freeze or no-freeze before x, whereas our main interest is in the probability of freezes after x. This is clearly one minus the probability obtained from (2). Let

$$H(x)=1-G(x),$$

then

$$H(x)=1-q_s-p_sF_s(x);$$

and since $p_s+q_s=1$,

$$H(x)=p_s[1-F_S(x)]. \tag{3}$$

If we write

$$I(x)=1-F_S(x) \tag{4}$$

equation (3) becomes

$$H(x)=p_sI(x). \tag{5}$$

This gives the probability of a freeze occurring after date x in spring.

For fall freeze we have a similar mixed distribution except that the probability of no-freeze is now concentrated after the fall freeze season and again does not enter into the probability before x. Hence the date distribution is

$$J(x)=p_aF_A(x) \tag{6}$$

Here p_a is the probability of a fall freeze and $F_A(x)$ is the distribution function on date. Since the distribution function gives the probability of freeze before date x, equation (6) gives the required probability directly. If the probability after x is needed, this may be obtained from $1-J(x)$. This then includes q_a, the probability of no-freeze in fall (autumn).

It should be noted that equations (5) and (6) hold generally, for in the situation where freeze occurs every year, as discussed in [1], $q=0$ and $p=1$.

3. ESTIMATION OF FREEZE PROBABILITIES

The main objective in developing the freeze distribution is to provide the means of obtaining probabilities. Thus, proper estimation of the terms in (5) and (6) will provide estimates of the required probabilities. There are two ways in which we can estimate these terms: Having estimated the p's, we may estimate the I and F_A functions directly from the data, or we may first estimate the parameters of the I and F_A functions. Before we can perform these estimations, however, we must define our climatological variable, freeze-date, more closely.

Clearly calendar date would be unsatisfactory as a variable. However, we can easily convert calendar date to day number beginning from some suitable base date. This will facilitate computations, the statistics from which may be readily converted back to calendar date. Since freeze dates vary over the periods July 1 to December 31 and January 1 to June 30, January 1 has been chosen as the base date. In leap years the 366-day year was employed.

Inasmuch as the base date will affect the mean of an incomplete freeze series, it might appear to be somewhat better to place the base date at a point halfway between the means of the fall and spring dates when freeze actually occurred. However, this would result in little refinement and would cause great inconvenience, for a computation of the halfway date would be required for each station. An examination of a number of stations showed that the halfway date usually occurs a few days after January 1. In view of the larger dispersion of the spring dates, the ideal base date, on probability considerations, should be displaced backward in time somewhat from the halfway date. This, together with the fact that the choice of base date does not greatly affect the probabilities, seemed to make the January 1 base the most satisfactory. All data with which we shall be concerned have therefore been coded to January 1. Tables 2, 3, and 4 show the freeze dates coded in this manner for Anniston, Birmingham, and Auburn, Ala. The data are arranged in order of increasing date and labeled with order number k. The three southern stations were chosen to emphasize the incompleteness aspect of the freeze series which is the central problem of the present analysis.

Our first estimates of H and J will be empirical or nonparametric. These involve first the estimation of I and F_A. While ordinarily with quite long series these would be estimated by k/m where k is the order number and m is the number of actual freeze dates, it has been found that for a continuous distribution the following equation gives estimates which are more unbiased at the smaller and larger probabilities:

$$F^*=\frac{k}{m+1}. \tag{7}$$

For spring this becomes

$$I^*=1-\frac{k}{m+1}. \tag{8}$$

TABLE 1.—*Statistics for various freeze thresholds for Anniston, Auburn, and Birmingham, Ala.*

Freeze	n	m	$\bar{x}$ (code)	$\bar{x}$ (date)	$\bar{u}$ and $\bar{v}$ (date)	s	$\hat{p}$	a	$\sqrt{b_1}$
ANNISTON									
Spring									
32	29	29	80.4	3/30	3/30	14.0	1.000	0.820	−0.195
28	29	29	70.1	3/11	3/11	16.9	1.000	.768	.005
24	29	28	55.0	2/24	2/22	18.0	.966	.779	−.846
20	29	26	47.0	2/16	2/11	19.2	.897	.816	−.375
16	29	16	39.8	2/9	1/22	18.8	.552	.736	.431
Fall									
32	28	28	310.3	11/6	11/6	12.1	1.000	0.795	0.310
28	28	28	323.8	11/20	11/20	12.2	1.000	.770	−.985
24	28	22	333.4	11/29	12/6	13.9	.786	.716	.888
20	28	14	338.1	12/4	12/18	10.7	.500	.829	.279
16	28	9	345.1	12/11	12/25	11.7	.321	.728	−.710
AUBURN									
Spring									
32	30	30	80.3	3/21	3/21	16.6	1.000	0.805	−0.219
28	30	30	59.5	3/1	3/1	18.1	1.000	.793	−.478
24	29	27	44.9	2/14	2/11	21.4	.931	.813	−.381
20	29	23	42.6	2/12	2/3	19.6	.793	.864	−.173
16	29	12	32.0	2/1	1/13	15.1	.414	.789	.244
Fall									
32	30	29	317.9	11/14	11/16	9.6	0.967	0.842	−0.203
28	30	27	333.1	11/29	12/2	11.4	.900	.725	.910
28	30	19	338.6	12/5	12/14	12.9	.633	.841	.468
20	30	10	340.1	12/6	12/23	11.3	.333	.807	−.194
16	30	6	347.0	12/13	12/27	11.3	.200	.738	−.266
BIRMINGHAM									
Spring									
32	30	30	77.6	3/19	3/19	16.3	1.000	0.764	−0.493
28	30	30	62.7	3/4	3/4	17.3	1.000	.770	.097
24	30	28	50.5	2/20	2/16	15.7	.933	.818	−.245
20	30	19	44.4	2/13	1/28	17.0	.633	.788	−.219
16	30	14	34.4	2/3	1/16	19.7	.467	.849	.170
Fall									
32	30	29	316.7	11/13	11/14	12.2	0.967	0.797	−0.019
28	30	28	334.7	12/1	12/3	14.3	.933	.825	.116
24	30	21	339.8	12/6	12/13	12.5	.700	.854	.362
20	30	12	342.1	12/8	12/22	11.0	.400	.790	−.531
16	30	8	346.5	12/13	12/26	11.5	.267	.819	−.135

The star indicates a nonparametric or distribution-free estimate of a parameter from a sample.

To complete the estimation of H and J, we must estimate p_s and p_a. Since the freeze, no-freeze series forms a discrete distribution the estimates are found from

$$\hat{p}=\frac{m}{n}, \tag{9}$$

where $\hat{p}$ is the parametric estimate of p, m is the number of years with freeze, and n is the number of years with freeze or no-freeze. The number of years with no-freeze is, of course, $n-m$.

The estimates p_s and p_a are shown in the $\hat{p}$ column of table 1. These were obtained by applying equation (9) to the m's and n's listed there. The statistics for all thresholds are given in table 1, although only Anniston 16°, Auburn 24°, and Birmingham 20° are discussed in full.

TABLE 2.—*Estimated probabilities of 16° freeze for Anniston after given dates in spring and before given dates in fall*

Spring

k	Date	x	I^*	$\hat{I}$	H^*	$\hat{H}$
1	1/ 7	7	0.941	0.959	0.519	0.529
2	1/11	11	.882	.937	.487	.517
3	1/16	16	.824	.896	.455	.486
4	1/25	25	.765	.782	.422	.432
5	1/28	28	.706	.732	.390	.404
6	1/31	31	.647	.681	.357	.376
7	2/10	41	.588	.472	.325	.261
8	2/10	41	.529	.472	.292	.261
9	2/11	42	.471	.452	.260	.250
10	2/13	44	.412	.409	.227	.226
11	2/19	50	.353	.291	.195	.161
12	2/19	50	.294	.291	.162	.161
13	2/27	58	.235	.166	.130	.092
14	2/28	59	.176	.154	.097	.085
15	3/ 4	63	.118	.107	.065	.059
16	3/10	70	.059	.054	.033	.030

Max $|d|=0.116$

Fall

k	Date	x	F^*	$\hat{F}$	J^*	$\hat{J}$
1	11/16	321	0.100	0.018	0.032	0.006
2	12/ 3	337	.200	.251	.064	.081
3	12/ 7	341	.300	.367	.096	.118
4	12/ 9	343	.400	.433	.128	.139
5	12/12	346	.500	.532	.161	.171
6	12/16	350	.600	.663	.193	.213
7	12/17	351	.700	.691	.225	.222
8	12/23	357	.800	.844	.257	.271
9	12/26	360	.900	.896	.289	.288

Max $|d|=0.082$

The I^* and $F_A{}^*$ are estimated by applying equations (7) and (8) to the k's and m's of tables 2, 3, and 4, giving the I^* and F^* columns of spring and fall freeze of those tables. From equations (5) and (6) it is seen that it is necessary to multiply the I^* and F^* by p_s and p_a, respectively, to obtain H^* and J^*, the nonparametric estimates of the mixed distribution. From table 1 we find for Anniston 16°, $p_s=0.552$ and $p_a=0.321$. Multiplying these, respectively, by the values of I^* and F^* from table 2 gives the H* and J* columns of the table. A similar calculation applies to tables 3 and 4. It is seen then that H^* gives the probability that a freeze occurs after date x in spring and J^* the probability that a freeze occurs before date x in the fall. From table 2 we see that the probability of a 16° freeze at Anniston after February 11 is 0.260, after March 10 it is only 0.033, or about 1 year in 30. The probability of a 24° freeze occurring before November 19 at Auburn is 0.063 from table 3, and of a 20° freeze after March 10 at Birmingham is also 0.063 from table 4. We do not recommend the nonparametric estimates for use in obtaining probabilities since we have a theoretical distribution as we shall see below. However, the empirical probabilities are necessary for judging the fit of the theoretical distribution so they are plotted in distribution function form as broken lines in figures 1, 2, and 3. If one desires to use the empirical or nonparametric probabilities, the recommended form of graph would be that shown in these figures.

TABLE 3.—*Estimated probabilities of 24° freeze at Auburn after given dates in spring or before given da'es in fall*

Spring

k	Date	x	I^*	$\hat{I}$	H^*	$\hat{H}$
1	1/ 1	1	0.964	0.980	0.897	0.912
2	1/ 2	2	.929	.977	.865	.910
3	1/15	15	.893	.918	.831	.855
4	1/17	17	.857	.903	.798	.841
5	1/24	24	.821	.834	.764	.776
6	1/28	28	.786	.785	.732	.731
7	2/ 1	32	.750	.726	.698	.676
8	2/ 1	32	.714	.726	.665	.676
9	2/ 3	34	.679	.695	.632	.647
10	2/ 8	39	.643	.606	.599	.564
11	2/ 9	40	.607	.591	.565	.550
12	2/11	42	.571	.552	.532	.514
13	2/12	43	.536	.536	.499	.499
14	2/13	44	.500	.516	.466	.480
15	2/19	50	.464	.405	.432	.377
16	2/19	50	.429	.405	.399	.377
17	2/23	54	.393	.334	.366	.311
18	2/28	59	.357	.255	.332	.237
19	2/28	59	.321	.255	.299	.237
20	3/ 1	60	.286	.239	.266	.223
21	3/ 3	62	.250	.212	.233	.197
22	3/ 4	63	.214	.198	.199	.184
23	3/ 8	67	.179	.149	.167	.139
24	3/11	70	.143	.119	.133	.111
25	3/13	73	.107	.102	.100	.095
26	3/14	73	.071	.093	.066	.087
27	3/20	79	.036	.055	.034	.051

Max $|d|$=0.102

Fall

k	Date	x	F^*	$\hat{F}$	J^*	$\hat{J}$
1	11/15	320	0.050	0.077	0.032	0.049
2	11/19	323	.100	.117	.063	.074
3	11/20	324	.150	.133	.095	.084
4	11/24	328	.200	.212	.127	.134
5	11/25	329	.250	.233	.158	.147
6	11/26	331	.300	.258	.190	.163
7	11/27	331	.350	.284	.222	.180
8	11/28	332	.400	.312	.253	.197
9	11/29	333	.450	.337	.285	.213
10	11/30	334	.500	.367	.317	.232
11	12/ 2	337	.550	.429	.348	.272
12	12/ 9	343	.600	.641	.380	.406
13	12/ 9	344	.650	.641	.411	.406
14	12/11	345	.700	.695	.443	.440
15	12/14	348	.750	.773	.475	.489
16	12/16	350	.800	.816	.506	.517
17	12/23	357	.850	.925	.538	.586
18	12/26	361	.900	.954	.570	.604
19	12/30	364	.950	.977	.601	.618

Max $|d|$=0.133

TABLE 4.—*Estimated probabilities of 20° freeze at Birmingham after given dates in spring or before given dates in fall*

Spring

k	Date	x	I^*	$\hat{I}$	H^*	$\hat{H}$
1	1/15	15	0.950	0.970	0.601	0.614
2	1/16	16	.900	.952	.570	.603
3	1/24	24	.850	.875	.538	.554
4	1/28	28	.800	.821	.506	.520
5	1/30	30	.750	.791	.475	.501
6	1/31	31	.700	.773	.443	.489
7	2/10	41	.650	.571	.411	.361
8	2/11	42	.600	.548	.380	.347
9	2/13	44	.550	.504	.348	.319
10	2/15	46	.500	.456	.317	.289
11	2/19	50	.450	.367	.285	.232
12	2/19	50	.400	.367	.253	.232
13	2/19	50	.350	.367	.222	.232
14	2/19	50	.300	.367	.190	.232
15	2/28	59	.250	.198	.158	.125
16	3/3	62	.200	.154	.127	.097
17	3/4	63	.150	.140	.095	.089
18	3/10	70	.100	.076	.063	.048
19	3/14	73	.050	.049	.032	.031

Max $|d|$=0.083

Fall

k	Date	x	F^*	$\hat{F}$	J^*	$\hat{J}$
1	11/15	320	0.077	0.021	0.031	0.008
2	11/24	328	.154	.109	.062	.044
3	11/29	333	.231	.215	.092	.086
4	12/ 2	337	.308	.302	.123	.121
5	12/ 6	340	.385	.433	.154	.173
6	12/ 8	342	.462	.504	.185	.202
7	12/11	345	.538	.606	.215	.242
8	12/15	349	.615	.736	.246	.294
9	12/16	350	.692	.764	.277	.306
10	12/16	350	.769	.764	.308	.306
11	12/21	355	.846	.877	.338	.351
12	12/22	356	.923	.894	.369	.358

Max $|d|$=0.121

Reed [5] and later Thom and Shaw [1] found that the normal distribution provided very good fits to freeze-date series under a wide range of conditions for the 32° and other thresholds for complete series; i.e., for $p=1$. The series, of course, tend to be more incomplete the farther south we go. This is also accompanied by a shift in the center of the distribution toward the colder season; i.e., toward winter from both fall and spring. This shift of the distribution center naturally causes some concern since the tails of the distributions on the winter end could begin to show the effect of boundedness, and hence departure from normality due to the decrease in time interval over which late fall and early spring freeze can range. This was also the reason for testing our theory on stations in a southern region where conditions are most stringent. To verify a part of our theory it is necessary to test the continuous component of the mixed distribution for normality which is fitted to the date of freeze in the series of actual freeze occurrences.

Probability tables used in [1] due to Geary [6] are again employed to test for normality. In these, a, the standardized mean absolute deviation from the mean, and $\sqrt{b_1}$, the standardized central third moment, are measures of kurtosis and skewness. These statistics are listed in table 1. Using the tables of [6] it was found that none of the a's are significant at the 0.10 probability level, and only the $\sqrt{b_1}$ (in italics in table 1) for 28° freeze in fall at Anniston is significant at the 0.02 level. The four largest values of $\sqrt{b_1}$ are individually significant at the 0.10 level but average near zero. Two of these are negative and two are positive; however, fall and spring each have a negative and positive value. This is in disagreement with what we would expect on the basis of the possible boundedness mentioned above which would cause negative skewness in fall and positive skewness in spring. We feel, therefore, that it is reasonable to assume that these larger values were a result of sampling and that, therefore, the normal distribution satisfactorily fits the continuous component of the mixed distribution of freeze occurrence and date.

508099—59——4

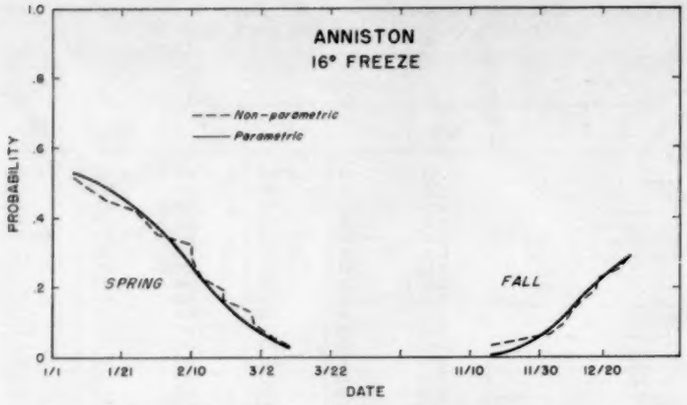

FIGURE 1.—Probabilities of 16° freeze at Anniston, Ala., occurring after any given date in spring or before any given date in fall.

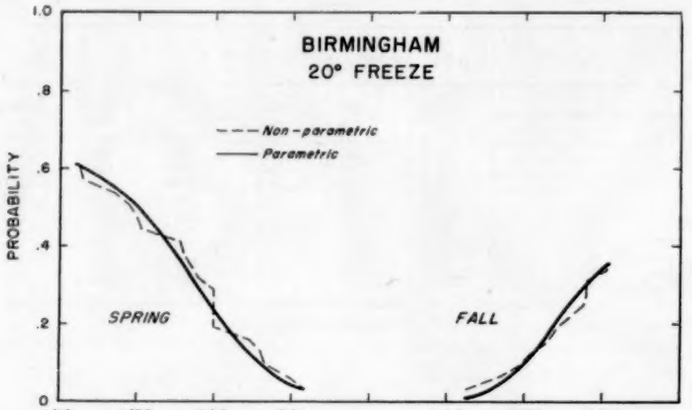

FIGURE 2.—Probabilities of 20° freeze at Birmingham, Ala., occurring after any given date in spring or before any given date in fall.

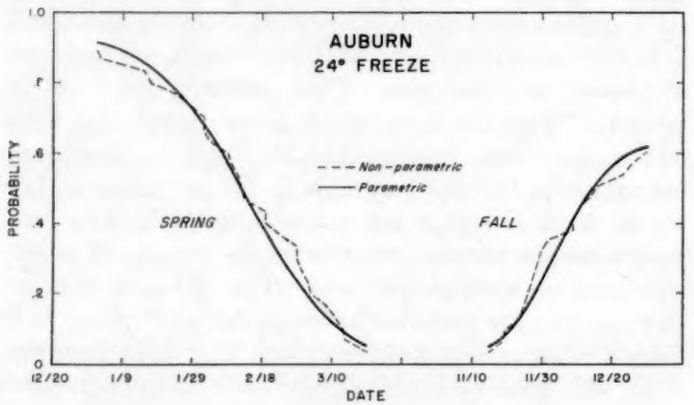

FIGURE 3.—Probabilities of 24° freeze at Auburn, Ala., occurring after any given date in spring or before any given date in fall.

$I(x)$ and $F(x)$ were fitted as normal distributions to the spring and fall freeze-date series in the usual manner by estimating the means and standard deviations. $I(x)$ gives the probability of freeze occurring after date x in spring and $F(x)$ the probability of an occurrence before date x in fall, both on the condition that freeze has actually occurred. These probabilities are parametric estimates and are indicated by $\hat{I}$ and $\hat{F}$ in tables 2, 3, and 4. The normal estimates and the nonparametric estimates of the probabilities may be compared by contrasting the careted and the starred distributions.

Although there is little question about the adequacy of the normal distribution in fitting freeze-date, it is of interest to test the fit in another manner. For this purpose we use the easily applied Kolmogorov-Smirnov test for which Massey has provided convenient tables. Massey [7] has also examined the power of the test and has found it superior to the χ^2 test in the cases analyzed. The test is carried out by examining the significance of

$$\max |d| = \max |k/m - \hat{I}(x)| . \qquad (10)$$

This is the maximum absolute difference between k/m and the normal distribution function. The maxima of $|d|$ are shown at the foot of each distribution table. Each value may, of course, be tested separately; however, we may test them all at once by considering the maximum of the max $|d|$ for the longest record employed in fitting the normal distributions. This will be a more stringent test than if we had used the actual length of record, length m. Max (max $|d|$) we see to be 0.133 and the longest record is 19 years. For these arguments Massey's table gives

$$P(\max |d| > 0.133) > 0.20$$

Since 0.20 is a rather large probability, the fit is good; in fact, all the fits are as good or better than this. This strengthens our conclusion of normality reached above. The goodness of fit also extends to the mixed distributions since there is little question of the fit of the p's.

The mixed distributions of spring and fall freeze are obtained from equations (5) and (6). These are the $\hat{H}$'s and $\hat{J}$'s of tables 2, 3, and 4 and are obtained from the $\hat{I}$'s and $\hat{F}$'s by multiplying respectively, by p_s and p_a. H^* and J^* are the nonparametric mixed distributions, and H and $\hat{J}$ are the parametric mixed distributions. These are plotted in figures 1, 2, and 3. Here one may observe the rather good fits of the smooth mixed theoretical distribution to the broken line empirical distributions. Probabilities of freeze before or after any date may be read from the smooth curves.

4. MEAN FREEZE DATE

Although the mean freeze date of the incomplete freeze series is more difficult to interpret, it is perhaps of some formal importance to consider it. Ordinarily the mean value of even a mixed distribution is obtained readily by

finding the expected value of the distribution. Here, however, the expected value depends on what value we assign to the dates on which we assume the probabilities q_s and q_a to be concentrated. We made some provision for this difficulty when we considered the freeze distributions above, but this was not as important there because the probabilities were not affected by the base date. If we make the reasonable assumption that the maximum growing season is 365 days, then it follows that when no-freeze occurs in spring, but one occurs at date x in fall, the growing season is x days long. If a freeze occurs at x in spring, but none occurs in fall, then the growing season is $(365-x)$ days long. We have previously chosen our day number code to give a reasonable interpretation to the mean dates; hence if we add our assumptions about growing season length, q_s will be assumed concentrated at code 0 and q_a at code $(365+0)$. 0 and $(365+0)$ are actually the same hypothetical day chosen so as to fit the conditions imposed by our model of the freeze-free season. We may now readily define the mean or expected values of the spring and fall freeze date.

For convenience we designate x_S and x_A as the continuous parts of the spring and fall freeze variables on the total interval $(1, 365)$ and x_a and x_s as the discrete parts. x_a only takes the value $(365+0)$ and x_s only the value 0. We define the pdf's on data in spring and fall to be $f(x_S)$ and $g(x_A)$, respectively. These are the derivatives of distribution functions expressed generally by equation (1). We need also to define the mixed variable date u for spring and v for fall, so as to include both the discrete and continuous parts. u and v then have the total range $(0, 365+0)$. With these additions, we may now express the mixed pdf of spring freeze by

$$h(u)=q_s+p_s f(x_S) \tag{11}$$

and for fall freeze by

$$j(v)=p_a g(x_A)+q_a. \tag{12}$$

The expected value or mean is defined as the sum and integral of the products of the variates by their probabilities. Taking into account the fact that q_s and q_a are discrete components of probability concentrated at 0 and $(365+0)$, we find the mean value for spring to be

$$E(u)=0\times q_s+p_s\int_S x_S f(x_S)dx_S \tag{13}$$

and for fall

$$E(v)=365q_a+p_a\int_A x_A g(x_A)dx_A. \tag{14}$$

Here S is the domain of spring freeze pdf and A is the domain of fall freeze pdf. Although in reality the domain $(S+A)$ is (1, 365) as mentioned previously, we find it convenient to assume S and A to be of infinite extent. This is plausible because the probability densities become very small near $x=1$, 365, and 364/2. With this assumption, together with the previous one that f and g are normal pdf's, it is clear that the integrals in (13) and (14) are mean values conditional on the occurrence of freeze. These may be expressed by $E(x_S)$ and $E(x_A)$ meaning the expected values in domains S and A. Equations (13) and (14) then reduce to

$$E(u)=p_s E(x_S) \tag{15}$$

and

$$E(v)=365\ q_a+p_a E(x_A). \tag{16}$$

Inasmuch as $E(x_S)$ and $E(x_A)$ are the means of normal distributions, they will be best estimated by the arithmetic means of spring and fall freeze dates $\bar{x}_S$ and $\bar{x}_A$. Substituting these estimates together with the estimates of the p's and q's, we find the estimated mixed means for spring

$$\bar{u}=p_s\bar{x}_S, \tag{17}$$

and for fall

$$\bar{v}=365\ q_a+p_a\bar{x}_A. \tag{18}$$

These are listed in table 1 for the stations studied and have been tabulated for a large number of Weather Bureau stations.

5. FREEZE-FREE SEASON DISTRIBUTION

It will be clear from our definition of the freeze-date variable for spring and fall that we may express the freeze-free season by the variable $y=v-u$. We shall assume, based on previous work for complete series [1], that spring and fall freeze dates are independently distributed. This seems all the more justified for incomplete freeze series since the spring and fall distributions are located farther apart in time than those for complete series. In order to find the distribution of freeze-free season, we must obtain the distribution of y. This may be most conveniently done by moment-generating functions or characteristic functions (cf). The former are ordinarily Laplace transforms and the latter Fourier transforms. It makes little difference which we use here since our development need only be a synthesis of known results. We prefer the cf because it has somewhat more general application.

The cf of a pdf is defined as the expected value of the Fourier kernel. (See [8], ch. 10.)

$$\varphi(t)=E(e^{itx})=\int_{-\infty}^{\infty} e^{itx} f(x)dx. \tag{19}$$

Here t is an arbitrary variable and $f(x)$ is the pdf. The analytical power of the cf arises from the fact that $\varphi(t)$ is a Fourier transform, and therefore the inverse may immediately be expressed as

$$f(x)=\frac{1}{\sqrt{2\pi}}\int_{-\infty}^{\infty}\varphi(t)e^{-itx}dt \tag{20}$$

which gives the required pdf. The cf's are obtained from the pdf's of equation (11) and (12) (see [8], pp. 57–58) by multiplying by the Fourier kernel and taking expected values. This gives

$$\varphi(t)=q_s+p_s\,\varphi_S(t) \tag{21}$$

and

$$\omega(t)=q_a+p_a\,\varphi_A(t) \tag{22}$$

For convenience in convolution we may take $y=v+(-u)$ in which case the variable $-u$ has the cf $\varphi_S(-t)$ ([8], p. 185), and we may rewrite (21) as

$$\zeta(t)=q_s+p_s\,\varphi_S(-t). \tag{23}$$

By the principle of convolution of distributions the cf of the sum $y=v+(-u)$ will be the product of (22) and (23); i.e.,

$$\Omega(t)=q_sq_a+q_sp_a\varphi_A(t)+q_ap_s\varphi_S(-t)+p_sp_a\,\varphi_A(t)\varphi_S(-t). \tag{24}$$

Assuming normal distributions for spring and fall freeze-date, we consider the last term first. This is the term involving freeze occurrence in both spring and fall. It is well known that the cf of a normal distribution with mean μ and standard deviation σ is

$$\omega(t)=\exp\left[-\tfrac{1}{2}t^2\sigma_A{}^2+it\mu_A\right] \tag{25}$$

using our variable for fall freeze. Hence for spring we have the required cf

$$\xi(t)=\exp\left[-\tfrac{1}{2}t^2\sigma_S{}^2-it\mu_S\right] \tag{26}$$

Multiplying (25) by (26), we find the cf of the mixture component of freeze-date to be

$$\omega\zeta=\exp\left[-\tfrac{1}{2}t^2(\sigma_A{}^2+\sigma_S{}^2)+it(\mu_A-\mu_S)\right] \tag{27}$$

Since this is of the form (25) with mean $\mu_A-\mu_S$ and variance $(\sigma_A{}^2+\sigma_S{}^2)$, it is a normal distribution with these parameters. We shall express the pdf of this cf as $w(z)$ where $z=(x_A-x_S)$.

As to the other terms on the right of equation (24), the first term is the product of the probabilities that there is no freeze in either spring or fall and is consequently the probability that the freeze-free season is 365 days. The pdf's of the second and third terms may be interpreted as follows: The second term is the mixture component with no-freeze in spring but one in fall; hence the variable $z=(x_A-0)=x_A$. Since the cf is for the pdf g, this remains $g(x_A)$. The third term of (24) is the mixture component with freeze in spring but none in fall. For this the freeze-free season variable is $z=365-x_S$ and the pdf becomes $f(365-x_S)$ which has the cf $\varphi_S(-t)$ with a location shift to account for our chosen freeze-date scale.

With these interpretations made, we may now write the pdf of freeze-free period as

$$q(y)=q_sq_a+q_sp_ag(x_A)+q_ap_sf(365-x_S)+p_sp_aw(z). \tag{28}$$

If we integrate equation (28) term by term, remembering that the first term is a constant, we find the distribution function of freeze-free period to be

$$Q(y)=q_sp_aF_A(x_A)+q_ap_sF_S(365-x_S)+p_sp_aW(z)+q_sq_a. \tag{29}$$

As we have seen previously, the distribution function gives the probability of an occurrence of freeze before date x; hence $Q(y)$ gives the probability of a growing season less than y. This may be obtained from equation (29) by substituting the estimates for the p's, q's, means $(\bar{x})$, and standard deviations (s) from table 1.

As an example, we obtain $Q(y)$ for the 16°−16° freeze-free period at Anniston. This cannot be expressed as a single function; it must be compiled by adding the component probabilities of equation (29). From table 1 we find the mean of the 16° fall-freeze variate to be $\bar{x}_A=345.1$ and the standard deviation $s_A=11.7$. According to our definition, the mean for the spring freeze variate is $365-\bar{x}_S$. From table 1, 16° spring freeze, we find $\bar{x}_S=39.8$; hence, $365-\bar{x}_S=325.2$. Since the standard deviation is not affected by either the algebraic sign of x_S or its subtraction from 365, s_S is also found from table 1 and is 18.8. From equation (27) we see that the sample mean of the last component is $\bar{z}=\bar{x}_A-\bar{x}_S=305.3$, and the standard deviation is

$$\sqrt{s_a{}^2+s_S{}^2}=\sqrt{(11.7)^2+(18.8)^2}=22.1.$$

From table 1 we also find $p_s=0.552$ and $p_a=0.321$. The q's are one minus the p's; hence $q_s=0.448$ and $q_a=0.679$. These readily yield the coefficients in (29): $q_sp_a=0.144$, $q_ap_s=0.375$, $p_sp_a=0.177$. The probability of a 16°–16° freeze-free season of 365 days is $q_sq_a=0.304$. Note that the coefficients of the probability function (28) add to unity as they should.

The probabilities for each component of the mixture for a convenient set of freeze-free season durations were computed using the above data and are listed in table 5. The theoretical distribution $\hat{Q}$ is listed in the eighth column and is the sum along rows of the three components. The empirical distribution Q^* computed from the original freeze-free season series by equations (7) and (29) is shown in the last column for comparison purposes.

The theoretical and empirical freeze-free distributions are shown in figure 4, the former by the smooth curve

TABLE 5.—*Distributions ($\hat{Q}$ and Q*) of freeze-free season durations for 16° threshold for Anniston, Ala., and probabilities for each component of the mixture*

y	$\hat{W}$	$\hat{F}_A$	$\hat{F}_B$	$\hat{p}_s\hat{p}_a\hat{W}$	$\hat{q}_s\hat{p}_a\hat{F}_A$	$\hat{q}_a\hat{p}_s\hat{F}_B$	$\hat{Q}$	y	F^*	Q^*
250	0.006			0.001			0.001	287	0.048	0.034
255	.011			.002			.002	288	.095	.068
260	.020			.004			.004	290	.143	.102
265	.034		0.001	.006			.006	295	.190	.136
270	.055		.002	.010		0.001	.011	301	.238	.170
275	.085		.004	.015		.002	.017	315	.286	.204
280	.127		.008	.022		.003	.025	315	.333	.238
285	.179		.016	.032		.006	.038	321	.381	.272
290	.245		.031	.043		.012	.055	323	.429	.306
295	.319		.054	.056		.020	.076	324	.476	.340
300	.405		.090	.072		.034	.106	324	.524	.374
305	.496		.142	.088		.053	.141	327	.571	.408
310	.583	0.001	.209	.103		.078	.181	337	.619	.442
315	.670	.005	.295	.119	0.001	.111	.231	337	.667	.476
320	.749	.016	.390	.133	.002	.146	.281	340	.714	.510
325	.813	.043	.496	.144	.006	.186	.336	341	.762	.544
330	.869	.099	.603	.154	.014	.226	.394	348	.810	.579
335	.910	.195	.698	.161	.028	.262	.451	351	.857	.612
340	.942	.330	.785	.167	.048	.294	.509	354	.905	.646
345	.964	.496	.853	.171	.071	.320	.562	357	.952	.680
350	.978	.663	.907	.173	.095	.340	.608			
355	.988	.802	.944	.175	.115	.354	.644			
360	.993	.898	.968	.176	.129	.363	.668			
365	.997	.955	.983	.176	.138	.369	.683			

and the latter by the broken line. The 365-day component of probability is the vertical line at right end of the theoretical curve. The maximum absolute difference between the empirical and theoretical curves, adjusted to unity to make the continuous part a distribution function, is 0.089. For sample size 20, the number years with freeze, Massey's [7] table gives a much larger value 0.231 at the 0.20 probability limit. The fit of the theoretical distribution to the actual data is therefore very good. Probabilities that the 16°–16° freeze-free season is less than any number of days read on the abscissa may be read from the ordinate of the figure.

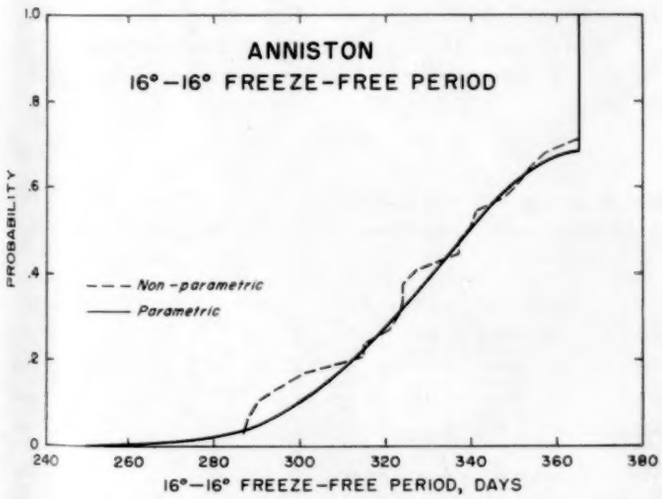

FIGURE 4.—Freeze-free distributions (16° threshold) for Anniston, Ala.

6. MEAN FREEZE-FREE SEASON

The mean or expected value of the freeze-free season which is at least of some formal interest can be readily found by the usual methods from equation (28). Multiplying each term by its variate and integrating, recalling that the first term is associated only with 365, and substituting rough values, we find

$$\bar{y}=365\,q_sq_a+q_sp_a\,\bar{x}_A+q_ap_s(365-\bar{x}_B)+p_sp_a\bar{z}. \quad (30)$$

It was pointed out to me by Dan Harton that $\bar{y}$ can obviously be obtained much more easily from the difference of equations (15) and (16). This gives

$$\bar{y}=365\,q_a+p_a\,\bar{x}_A-p_s\,\bar{x}_B. \quad (31)$$

By a considerable amount of algebraic manipulation, equation (30) may be reduced to equation (31). This is of interest since it shows that convolution has produced a distribution (28) consistent with the basic assumptions as, of course, it must if it is correctly defined.

Using either formula together with the values found above, we find $\bar{y}$, the mean 16°–16° freeze-free season at Anniston, to be 336.6 days. The means of spring and fall freeze and freeze-free period are available from Weather Bureau State climatologists for a large number of stations in the United States.

ACKNOWLEDGMENTS

The writer is indebted to Miss Ethel A. Taylor of the Agronomy Department, Cornell University, for performing the original computations, and to Professor Walter T. Federer of Cornell University for arranging the visiting

professorship which made this work possible. My assistant, Mr. Maurice Kasinoff, revised many of the computations to fit newer data, and Mr. Dan Harton, formerly of the National Weather Records Center, checked much of the algebraic work and devised programs for machine tabulation. Mr. Warren W. Buck, Jr., prepared the illustrations.

REFERENCES

1. H. C. S. Thom and R. H. Shaw, "Climatological Analysis of Freeze Data for Iowa," *Monthly Weather Review*, vol. 86, No. 7, July 1958, pp. 251–257.
2. W. J. Spillman, H. R. Tolley, and W. G. Reed, "The Average Interval Curve and Its Application to Meteorological Phenomena," *Monthly Weather Review*, vol. 44, No. 4, Apr. 1916, pp. 197–200.
3. H. C. S. Thom, "The Distribution of Freeze-Date and Freeze-Free Period When a Probability of No-Freeze Exists," *BU–30–M*, Biometrics Unit, Cornell University (mimeograph), 12 pp.
4. H. C. S. Thom, "Probabilities of One-Inch Snowfall Thresholds for the United States," *Monthly Weather Review*, vol. 85, No. 8, Aug. 1957, pp. 269–271.
5. W. G. Reed, "The Probable Growing Season," *Monthly Weather Review*, vol. 44, No. 9, Sept. 1916, pp. 509–512.
6. R. C. Geary and E. S. Pearson, "Tests of Normality," Separate No. 1, from *Biometrika*, vols. 22, 27, 28, Biometrika Office, University College, London, W.C. 1, 1938.
7. F. J. Massey Jr., "The Kolmogorov-Smirnov Test of Goodness of Fit," *Journal of the American Statistical Association*, vol. 46, 1951, pp. 68–78.
8. Harold Cramér, *Mathematical Methods of Statistics*, Princeton University Press, Princeton, 1946.

THE LOWEST TEMPERATURE IN ANTARCTICA

NINA A. STEPANOVA

Office of Climatology, U.S. Weather Bureau, Washington, D.C.

[Manuscript received April 17, 1959]

The IGY period 1957–58 was the first time in history that continuous meteorological observations were made in the interior of Antarctica. The U.S. IGY Amundsen-Scott Station (90° S., elev. 2,800 m.) and the Soviet IGY stations, Vostok (78°27′ S., 106°52′ E., elev. 3,420 m.) and Sovetskaya (78°24′ S., 87°35′ E., elev. 3,570 m.) are located on a high plateau of the Antarctic Continent and the minimum temperatures observed there have set new world records. In fact, the Antarctic winter season of 1958 saw a continuous breaking and resetting of the world minimum temperature record. As it now stands, the −87.4° C. (−125.3° F.) recorded at Vostok on August 25 is the world record.

Now that this eventful winter is over, the still fragmentary information from Antarctica can be analyzed and summarized. However, a reservation must be made as to the reliability of sources of this information. We are compelled to resort to a practice usually avoided in scientific analysis; that is, to a utilization of newspaper and radio reports. At this early date these are our only sources for some of the data which may be long in reaching publication in technical journals.

In a previous article [1] on the lowest temperatures reported on earth, we published the then latest record low air temperature for the world. It was −74.5° C. (−102.1° F.) observed at the U.S. Antarctic station at the South Pole (elev. 2,800 m.) on September 17, 1957. This minimum broke the previous record of −67.7° C. (−89.9° F.) observed at Oimekon in eastern Siberia on February 6, 1933. Carrying on from where we left off in the previous article, we show in table 1 a chronological list of the later world-record-breaking minima observed in Antarctica during the winter of 1958.

The new record of −87.4° C. has exceeded a theoretical estimate of the lowest possible Antarctic temperature made by Shliakhov [2]. His estimate was based on the assumption that radiation balance becomes zero at the theoretical minimum temperature; i.e., the back radiation from the atmosphere equals the upcoming radiation from the surface. Using actual radiation measurements from Vostok 1 and theoretical values derived from soundings made at Vostok 1 in May 1957 and at the South Pole in July 1957, and using the Shekhter radiation nomogram [3], Shliakhov computed the minimum temperature to vary from −78°±2° C. to −80°±1° C. He then performed another calculation based on greater station elevation (5 km. m.s.l.) and using a mean lapse rate of 5° C. per 1,000 m. above the inversion layer as determined from radiosoundings made at the interior stations. He assumed the temperature of the snow surface to be −75° C., the strength of the inversion −30° C., the depth of the inversion layer 1 km., and also assumed that

TABLE 1.—*Temperature minima observed in Antarctica since 1957*

Station	°C.	°F.	Date	Source
Amundsen-Scott Station (South Pole)	−74.5	−102.1	Sept. 17, 1957	E. C. Flowers and R. A. McCormick, "World Record Low Temperature, South Pole, September 17, 1957," *Monthly Weather Review*, vol. 85, No. 11, Nov. 1957, p. 383.
Vostok	−78	−108.4	May 3, 1958	*Priroda*, Moscow, Aug. 1958, p. 82.
Sovetskaya	−79	−110.2	May 9, 10, 1958	Do.
Vostok	−81	−113.8	June 15, 1958	*Izvestiia*, Moscow, July 2, 1958.
Sovetskaya	−81.2	−114.2	June 19, 1958	Do.
Vostok	−81.4	−114.5	July 24, 1958	*Vodnyi Transport*, Moscow, July 29, 1958.
Sovetskaya	−83	−117.4	July 25, 1958	Do.
Vostok	−85.5	−121.9	Aug. 7, 1958	*Vodnyi Transport*, Moscow, Aug. 19, 1958.
Vostok	−85.8	−122.4	Aug. 8, 1958	M. J. Rubin, "World Record Low Temperature," *Monthly Weather Review*, vol. 86, No. 8, Aug. 1958, p. 308.
Sovetskaya	−86.7	−124.1	Aug. 9, 1958	M. J. Rubin, "World Record Low Temperature," *Monthly Weather Review*, vol. 86, No. 8, Aug. 1958, p. 308.
Vostok	−87.4	−125.3	Aug. 25, 1958	*TASS*, Moscow, radio broadcast. *The New York Times*, Aug. 26, 1958. *Izvestiia*, Moscow, Aug. 1958. E. S. Rubinstein, "K Voprosu o Poliusakh Kholoda" (On the Problem of the Cold Poles), *Meteorologiia i Gidrologiia*, No. 12, 1958, pp. 28–30. E. M. Dobryshman, "Opredekenie Minimal'noi Temperatury v Antarktike" (Determination of the lowest temperature in Antarctica), *Meteorologiia i Gidrologiia*, No. 1, 1959, pp. 21–22. A. F. Treshnikov, *Zakovannyi v Led* (Icebound), Gosudarstvennoe Izdatel'stvo Geograficheskoi Literatury, Moscow, 1959.

the air was saturated in all layers. Calculating the back radiation of the atmosphere (E') from the Shekhter radiation nomogram and the corresponding equilibrium temperature (T_o), he found: $E'=0.100\pm0.005$ cal./cm.^{2}/min., and $T_o=-85°\pm2°$ C. at 5 km. above sea level. Taking into account the above estimated lapse rate, Shliakhov came to the conclusion that, at the height of about 4 km., in Antarctica the lowest temperature could not be below $-80°\pm2°$ C. At higher levels it could be lower by 0.5° per 100 m.

The early low minima of May and June 1958 seemed to bear out this calculation, but the final record was 5.4° lower than the predicted limit. In the following note, Dr. Wexler attempts to explain why the theoretical minimum temperature was too high.

REFERENCES

1. Nina A. Stepanova, "On the Lowest Temperatures on Earth," *Monthly Weather Review*, vol. 86, No. 1, Jan. 1958, p. 6–10.
2. V. I. Shliakhov, "O Minimal'nykh Temperaturakh v Antarktide" (On Minimum Temperatures in Antarctica), *Meteorologiia i Gidrologiia*, No. 4, 1958, pp. 5–7.
3. F. M. Shekhter, "O Vychislenii Radiatsionnogo Teplovogo Potoka v Atmosfere" (On Calculations of the Radiational Heat Flux in the Atmosphere), *Trudy*, Glavnaia Geofizicheskaia Observatoriia, vol. 22, 1950, p. 84.

NOTE ON LOWEST ANTARCTIC TEMPERATURE ESTIMATED BY SHLIAKHOV

H. WEXLER
U.S. Weather Bureau, Washington, D.C.
[Manuscript received May 4, 1959]

In the preceding note, Miss Stepanova referred to Shliakhov's estimate of lowest Antarctic temperature [1] which has been proven too high by subsequent events. It appears that the basic error committed by Shliakhov is in the association of a zero radiation balance with a certain temperature—the theoretical minimum. This is not true within the likely range of atmospheric temperatures because of the water-vapor absorption spectrum with its "window" near the maximum of the black-body radiation spectrum. As explained in an earlier paper [2], although the surface temperature may reach a state of "quasi-radiative equilibrium" wherein the back atmospheric radiation exactly equals the upcoming radiation from the surface, the surface temperature continues to fall for the following reason: All of the back radiation from the atmosphere is absorbed by the snow surface which acts as a black-body for infrared radiation but not all of the upcoming radiation is absorbed by the atmosphere which is not a black-body. Consequently there is a net loss of energy in the atmosphere which cools and then sends less back radiation to the surface, which then cools also, and so on.

Shliakhov essentially attempts to calculate this effect and comes to the conclusion that it could only change the temperature of the lowest 3 km. by 1° C. in 200 hours, or 8.4 days, and neglects it in the calculation of the theoretical minimum temperature. But as the data in Stepanova's table 1 show, the succession of minimum temperatures proceeds so slowly with time that a cooling rate of 1° C. per 8.4 days cannot be neglected.

McCormick [3] has shown that in the absence of advective and conductive processes the theoretical minimum could be −200° C. in 180 sunless days at the South Pole.

REFERENCES

1. V. I. Shliakhov, "O Minimal'nykh temperaturakh v Antarktide" (On Minimum Temperatures in Antarctica), *Meteorologiia i Gidrologiia*, No. 4, 1958, pp. 5–7.
2. H. Wexler, "Cooling in the Lower Atmosphere and the Structure of Polar Continental Air," *Monthly Weather Review*, vol. 64, No. 4, April 1936, pp. 122–136.
3. R. A. McCormick, "An Estimate of the Minimum Possible Surface Temperature at the South Pole," *Monthly Weather Review*, vol. 86, No. 1, Jan. 1958, pp. 1–5.

A NOTE ON VISIBILITY AT SACRAMENTO, CALIF.

GEORGE C. HOLZWORTH

Weather Bureau Research Station, Berkeley, Calif.

[Manuscript received January 13, 1959]

ABSTRACT

Daylight visibility observations at the Sacramento Municipal Airport were used to investigate the possibility that visibility in the area has been declining due to rising levels of air pollution. Those visibility observations made with naturally occurring fog (defined as relative humidity greater than 90 percent) and/or precipitation were eliminated from the data. Observations for July, a warm, dry month with relatively slight climatic differences from year to year, and November, a cool month that often exhibits a considerable annual variation of climate, were tabulated for the three 4-year periods, 1935–38, 1945–48, and 1953–56. The results show that for July the percent frequency of poor visibilities steadily increased, and of good visibilities steadily decreased over the last 20-odd years. Such a trend is consistent with the Sacramento population increase. For November the trend was irregular. This is believed to be due to variations in the occurrence of meteorological factors important to atmospheric dispersion. It is likely that such irregularities are characteristic of other months and areas where there are large annual climatic variations.

From concurrent surface wind observations, the preferred wind conditions for various visibility ranges were determined. These data indicate that poor visibilities at the airport, on the southern edge of the city, occurred most frequently with light winds from over the nearby Sacramento urban area. Good visibilities were favored by moderate winds from rural directions. Visibilities were reduced when the wind speed became strong enough for loose materials to be picked up from the ground.

1. INTRODUCTION

Residents of Sacramento and other cities in California's Central Valley, as well as aircraft pilots in the vicinity, have stated that over the years they have observed a general decrease in visibility. These individuals have attributed such a trend to increasing levels of air pollution. Because air pollution measurements have not been made in the Central Valley until recently, studies of trends in the concentrations of specific pollutants are not possible. However, the solid and liquid particulate matter suspended in the atmosphere, which represents air pollution, reduces visibility [1], and therefore a measure of visibility may be interpreted as a measure of air pollution. Hence, changes in visibility not attributable to naturally occurring aerosols may be indicative of manmade trends in air pollution. This study was undertaken in order to assess the possibility that there has been a general deterioration of visibility in the Sacramento area due to human activity.

2. DATA AND TREATMENT

From the hourly weather observations made by the U.S. Weather Bureau at Sacramento Municipal Airport, the July and November data for the three 4-year periods 1935–38, 1945–48, and 1953–56 were selected and punched on cards for machine tabulation. Only daytime observations, 0730–1730 PST,[1] were considered since visibility at night depends upon different factors and the observations are generally less reliable [1]. All observations, 1935–56, were made from the same location.

Prior to 1943 visibility to be reported by Weather Bureau observers was defined as "the greatest distance toward the horizon that known objects can be identified." This was later revised to "the lowest visibility over the half of the horizon with the greatest visibility." Summaries for this study do not suggest that this change in definition had any noticeable effect on Sacramento observations.

July and November visibility trend analyses were considered with respect to the three 4-year periods. The data were lumped into 4-year groups in an attempt to smooth out year-to-year variations in meteorological conditions such as factors affecting the dispersion of pollutants.

The natural aerosols which limit visibility are fog and precipitation. Precipitation may occur at various relative

[1] Actual observation times are about 28 minutes past the hour for 1945–56 and about 41 minutes past the hour for 1935–38. At Sacramento in November the latest sunrise is about 0700 PST and the earliest sunset is near 1700 PST.

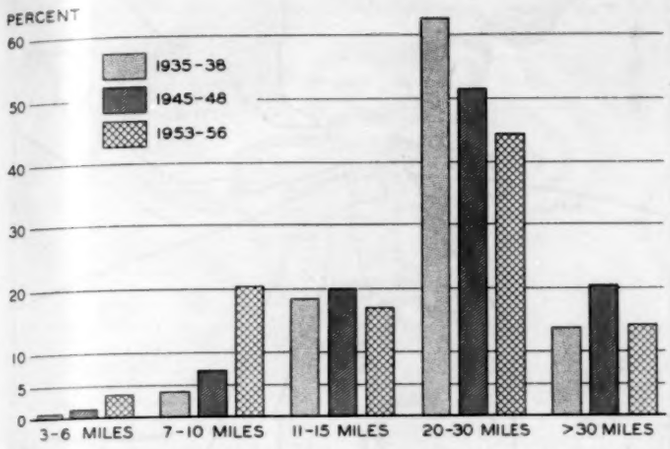

FIGURE 1.—July visibilities at Sacramento Municipal Airport, 0730–1730 PST. Percent frequencies when relative humidity less than 91 percent and no precipitation occurring.

humidities, but natural fog is unlikely below about 91 percent. Those visibility observations with precipitation and/or relative humidity greater than 90 percent were tabulated separately, and remaining visibility observations were originally broken down according to various other relative humidity ranges. Although the visibilities tended to be lower with higher humidities, the trends between 4-year periods for various humidity ranges were all similar. For this reason, and because it is desirable to deal with large samples, all visibilities recorded with humidities below 91 percent (and no precipitation) were considered together. In 96.7 percent of the July visibility cases, humidities were less than 71 percent. In November, humidities were below 71 percent in 60.2 percent of the cases and below 91 percent in 83.9 percent of the cases.

3. RESULTS

In the following discussions visibility observations with precipitation and/or relative humidity greater than 90 percent are excluded. This provision is intended to eliminate visibility restrictions that might be attributed to naturally occurring fog and precipitation particles.

JULY

July was chosen as typical of the warm, arid summers when there are seldom marked variations in Central Valley weather. The percent frequencies of visibilities in given ranges for each of the three 4-year periods are shown in figure 1. This bar diagram indicates that the frequency of visibility reports in the ranges 3–6 and 7–10 miles steadily increased over the years studied. The percentage frequency of the combined 3–10-mile range increased by a factor of almost 5 from 1935–38 to 1953–56, apparently at the expense of the 20–30-mile range whose frequency

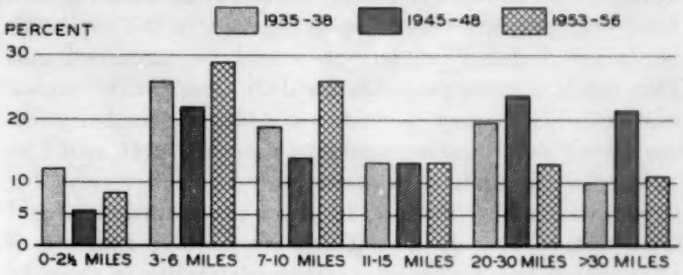

FIGURE 2.—November visibilities at Sacramento Municipal Airport, 0730–1730 PST. Percent frequencies when relative humidity less than 91 percent and no precipitation occurring.

steadily declined from 62.8 percent in 1935–38 to 44.5 percent in 1953–56. The frequency of visibilities of 11–15 miles changed only slightly and inconsistently with time. In the range exceeding 30 miles, there was no regular trend. There were no July visibilities of 0–2½ miles. Considering all visibilities, a deteriorating trend is clearly indicated for July.

The most striking visibility trends were in the 3–10- and 20–30-mile ranges. By the chi-square test [2], differences between the three 4-year periods for both these visibility ranges are significant at the 1-percent level. It should be mentioned that such tests of significance assume independence of samples, and hourly weather observations do not fully satisfy this assumption. However, each of the 4-year groups was considered to more clearly approach the property of independence.

NOVEMBER

Climatologically, November is a relatively cool month and was chosen to represent early winter conditions as opposed to summer. The weather is often quite variable within this month and considerable differences may occur from year to year. Some Novembers are rainy and foggy while others are relatively dry and fog free.

The percentage frequencies of visibilities in given ranges for each of the three 4-year periods, as shown in figure 2, indicate that November visibilities followed an irregular trend. As a whole, poor visibilities (0–10 miles) were least frequent, and good visibilities (20 miles or greater) were most frequent in the middle period, 1945–48. In the later period, 1953–56, the picture was reversed with 0–10-mile visibilities most frequent and visibilities of 20 miles or greater least frequent. In the early period, 1935–38, poor and good visibilities occurred with frequencies intermediate between those of the other two periods. The frequency of visibilities of 11–15 miles differed between periods by only 0.2 percent. Considering all visibilities for November, they may be described as having been intermediate in 1935–38, good in 1945–48, and poor in 1953–56.

This irregular variation stands in sharp contrast to the steady trend shown for July. As mentioned above, data for 4-year periods were lumped together in the hope that important weather variations would be smoothed out. This result is more probable for July than for November when conditions may be quite variable. November average 4-year precipitation amounts were 1.09, 1.41, and 1.59 inches for the earliest to latest periods, respectively; for any one November in these 12 years, precipitation ranged from 0.03 to 3.35 inches. These are cited to indicate to some extent the degree of weather variability in these 12 Novembers. It is thought that such variations in important meteorological factors, affecting both dispersion and emission of visibility-reducing pollutants, have resulted in the irregular November trend shown in figure 2.

With respect to pollutant sources, the burning of crop residues after harvesting should be mentioned. It is thought that this practice, which has been common in the rich agricultural area of Sacramento and other parts of the Central Valley, is partly responsible for the irregular trend of November visibilities. Smoke from what agricultural burning occurs in July is likely to be more rapidly dispersed by the usual summer conditions of windiness and instability. However, because the desired facts on agricultural burning are nonexistent, such remarks must be regarded as speculation.

4. FURTHER CONSIDERATION

It is generally recognized that as urban areas expand, pollutant emissions from such sources also increase (in the absence of emission controls). It is logical then that, other things being the same, visibility should show a general decline with increasing urbanization. The Sacramento Municipal Airport is on the southern edge of the city, about 4½ miles from the downtown area. Because Sacramento is the only large city in the county and because much of the total metropolitan population lies beyond the official city limits, Sacramento County population figures have been used. From decennial population data [3] and others [4], the following population estimates were made for Sacramento County for 1 year within each of the three periods studied:

1937	160,000
1947	230,000
1955	380,000

Thus the trend of deteriorating July visibilities was associated with a rapidly increasing population. In November this same trend held true for 1945–48 to 1953–56, but improving visibilities from 1935–38 to 1945–48 were also associated with a population increase. As pointed out, this latter irregularity is believed to have been due to variations of important meteorological factors.

That the Sacramento metropolitan area was indeed a source of visibility-reducing pollutants may be shown from

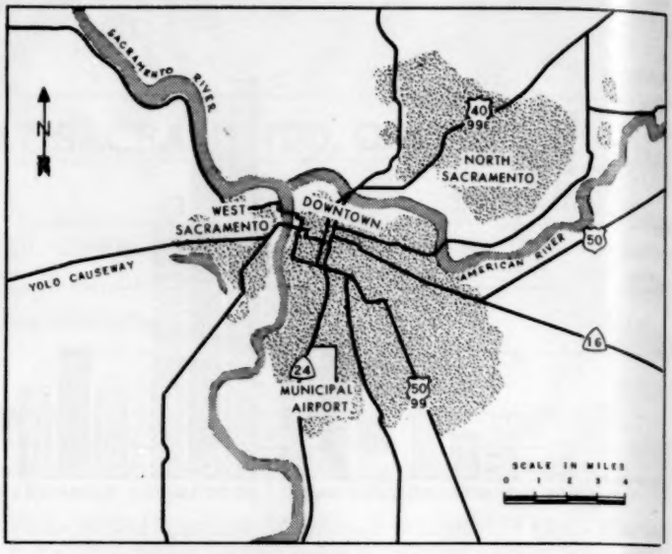

FIGURE 3.—Schematic map of Sacramento, Calif.

a consideration of surface winds. For each visibility observation the concurrent wind observation was tabulated in wind rose form for each visibility range. Wind directions were divided into two groups, northwest clockwise through east-southeast (NW–ESE) and southeast through west-northwest (SE–WNW). As shown in figure 3, most of the Sacramento metropolitan population lies in the sector NW–ESE from the airport. The other sector, SE–WNW, may be described as relatively rural. The relationship of poor visibilities (0–10 miles) to winds was considered first. This was done by summarizing the percent frequency of occurrence of wind in each of the two direction sectors, NW–ESE and SE–WNW, by 5-m.p.h. speed intervals for 0–10-mile visibilities and for all visibilities. The ratio of the former to the latter was then determined and these values for July and November are given in table 1. Each number in this table is the ratio of percent frequency of given wind conditions for low visibility to the percent frequency of such wind conditions for all visibilities. Thus, the higher the ratio, the greater the "preference" of low visibilities for such wind conditions.[2] For example, table 1 shows that in July the most preferred wind condition for 0–10-mile visibilities was from NW–ESE at 1–5 m.p.h. It should be made clear that these wind conditions are not necessarily those with which the visibility was most often 0–10 miles. The preference is relative to what is expected from a consideration of all visibilities.

[2] Using tables B and F of *Local Climatological Data Supplement*, it is possible to compute the ratios of "percent of time the wind is from given directions for visibilities less than 7 miles with smoke or haze" to "percent of time the wind is from corresponding directions for all visibilities."

TABLE 1.—*Ratio of "percent of winds for visibility 0–10 miles" to "percent of winds for all visibilities." Data for Sacramento Municipal Airport when relative humidity less than 91 percent and no precipitation; 0730–1730 PST, 1935–38, 1945–48, 1953–56*

Wind speed m.p.h.	Wind direction			
	NW-ESE	SE-WNW	Calm	All
JULY (No visibility reported in 0–2½ miles range)				
Calm			2.57	2.75
1–5	3.03	1.82		2.12
6–10	1.49	.96		1.05
11–15	.80	.43		.45
16–20	2.23	.44		.50
>20	None	.77		.77
All	1.90	.83		
NOVEMBER				
Calm			1.49	.49
1–5	1.36	1.16		1.27
6–10	1.04	.88		.98
11–15	.27	.52		.41
16–20	.18	.36		.25
>20	.47	.36		.44
All	.99	.89		

TABLE 2.—*Ratio of "percent of winds for visibility 20–30 miles" to "percent of winds for all visibilities". Data for Sacramento Municipal Airport when relative humidity less than 91 percent and no precipitation; 0730–1730 PST, 1935–38, 1945–48, 1953–56*

Wind speed m.p.h.	Wind direction			
	NW-ESE	SE-WNW	Calm	All
JULY				
Calm			0.75	0.75
1–5	0.68	0.79		.77
6–10	.86	.95		.94
11–15	1.33	1.14		1.15
16–20	1.50	1.14		1.14
>20	1.86	1.10		1.12
All	.89	1.02		
NOVEMBER				
Calm			0.34	0.34
1–5	0.51	0.88		.67
6–10	1.01	1.17		1.08
11–15	1.33	2.30		1.86
16–20	.84	2.92		1.67
>20	1.03	2.50		1.41
All	.83	1.39		

Wind speeds exceeding 15 m.p.h. were infrequent, and so the ratios for such speeds had to be computed from small percentages. However, the computed ratios appear to exhibit reasonable trends as wind conditions vary. A likely exception is the value of 2.23 in table 1, July, which probably would be lower with more cases of such winds. This fault might be corrected by combining some of the higher wind speeds, but in so doing one of the features of the table would be lost. It is a reasonable hypothesis that, considering nearby community sources of visibility-reducing aerosols, improving visibility should be anticipated with increasing wind speed (more favorable dilution) up to the point where dust and other loose materials are picked up by the wind. This is borne out in table 1 where, considering all wind directions, there is a decrease in the ratios with increasing speeds up to the point where loose material is picked up. Here the ratios begin to increase. In July when precipitation averaged less than a trace and the ground was dry, this reversal began at 16–20 m.p.h. In November when precipitation averaged 1.36 inches, the ratios did not begin to increase until speeds exceeded 20 m.p.h.

From table 1 it is clear that wind directions occurring with low visibilities were most likely to be from the urban area. This was especially true for July when for every wind speed the ratios were greater for the sector NW–ESE than for the SE–WNW sector. For November, considering all wind speeds, the most preferred direction with low visibilities was also from the metropolitan area. However, the preference was not nearly so strong as in July. This may have been due in part to agricultural burning which provides pollutant sources to the south as well as to the north.

Table 2 is similar to table 1 except it is for good visibilities, 20–30 miles. This table indicates that for all directions there was an increase in the ratios, preference for good visibilities, with increasing speeds up to the point where loose materials are picked up, and then the trend reversed. Considering all wind speeds, the most preferred direction for good visibility was from the rural sector, SE–WNW.

Hygroscopic nuclei may be active in the humidity range 71–90 percent. If such relative humidities are related to wind directions, then the concurrent visibilities might be lower and tables 1 and 2 would be invalid. July daytime humidities above 70 percent are very rare. In November, humidities of 71–90 occurred 23.7 percent of the time. The November ratios in tables 1 and 2 were recomputed, using only data for relative humidities below 71 percent (and no precipitation). The recomputed ratios are almost identical with the original. It is concluded that any relationship between humidities of 71–90 percent and wind directions does not alter the ratios of tables 1 and 2.

5. CONCLUSIONS

The data for July indicate that Sacramento visibilities have been deteriorating over the last 20-odd years. This is most apparent in the 0–10-mile visibility range, which showed a steady increase in percent frequency, and in the 20–30-mile range, which showed a steady decrease. In November, visibilities went through an irregular trend from intermediate to good to poor, from the earliest to the latest periods, respectively. This may have been due

largely to variations in the occurrence of meteorological factors, especially those important to atmospheric dispersion of manmade pollutants. It is likely that such irregularities are characteristic of other seasons and areas where there are large variations in the weather.

From a consideration of wind data it is clear that poor visibilities were associated with wind directions from over the urban area and with light winds. Wind direction and speed factors were interdependent. Good visibilities were most likely with winds from rural directions and at moderate speeds. The data indicate that visibilities were reduced when winds became strong enough to pick up dust and other loose materials.

ACKNOWLEDGMENTS

This work was carried out in cooperation with the California State Department of Public Health as a part of the program of the Bureau of Air Sanitation. Various people in this Bureau made helpful suggestions and their contributions are gratefully acknowledged.

The raw data were kindly made available by the U.S. Weather Bureau at Sacramento. The encouragement of the Office of Meteorological Research and the Weather Bureau Research Station at the R. A. Taft Sanitary Engineering Center, Cincinnati, Ohio, is also appreciated.

REFERENCES

1. H. G. Houghton, "Visibility," *Handbook of Meteorology*, McGraw-Hill Book Co., Inc., New York, 1945, pp. 242–251.
2. H. A. Panofsky and G. W. Brier, *Some Applications of Statistics to Meteorology*, Pennsylvania State University, University Park, Pa., 1958, see pp. 53–58.
3. U.S. Bureau of the Census, Census data for 1930, 1940, 1950.
4. California State Department of Finance, Population estimate for 1956.

THE WEATHER AND CIRCULATION OF APRIL 1959

Including the Role Played by an Index Cycle

JAMES F. ANDREWS

Extended Forecast Section, U.S. Weather Bureau, Washington, D.C.

1. INTRODUCTION

April 1959 was characterized by a lack of severe local storminess throughout most of the United States. A similar condition prevailed in April of 1958 [1], in sharp contrast to the stormy April of 1957 [2] when a record number of tornadoes was observed. From the northern Rocky Mountain States southeastward to the Gulf States, temperatures averaged below the seasonal normals, while west of the Rockies and in the northeastern third of the Nation the weather was generally mild. The long period of unusual warmth continued along the California coast, with new April temperature records being established. Precipitation continued deficient in the northern Great Plains and upper Mississippi Valley, with some areas reporting the least amount of record for the period January to April. Subnormal amounts of precipitation also fell in parts of the Southwest, thus continuing the dryness of the winter season.

Despite the fact that few monthly records were established during April, pronounced changes in weather and circulation did occur. These changes can be related to a strong index cycle.

2. MONTHLY MEAN CIRCULATION

The average circulation pattern for April 1959 (fig. 1) was one of relatively fast westerly flow with wave systems of small amplitude around the entire Northern Hemisphere. Over the Western Hemisphere the zonal index, a measure of the net geostrophic west wind between latitudes 55° N. and 35° N., averaged 0.8 m.p.s. above the April normal. This continues the period of above normal values of this index that began in February 1959 [3]. At higher latitudes the polar westerlies (55° N.–70° N.) were 0.8 m.p.s. below normal, mostly as a result of blocking over eastern Canada. The subtropical westerlies (20° N.–35° N.) also averaged slightly below their normal value.

Only one full-latitude trough was observed during April, from the Bering Sea southward to just west of the Hawaiian Islands (fig. 1). Nearly-full-latitude troughs were observed along the eastern Asiatic coast and over eastern North America. The latter trough, along with a strong ridge over the Pacific coast, controlled much of the weather in the United States. Blocking in Scandinavia was associated with a middle- and low-latitude trough extending from eastern Europe to North Africa. The latter two features of the planetary circulation resulted in confluence over central Asia, where a narrow band of above normal wind speeds prevailed at 700 mb.

In the Pacific the zone of maximum wind speed at 700 mb. was found just east of the Japanese Islands (fig. 2A), somewhat farther west than normal. This position can be related to the westward displacement of the normal trough near the Asiatic coast [4] and to the appearance of a mean ridge in the western Pacific (fig. 1).

Across North America the major trough-ridge system was also displaced west of its position on the normal map [4], though wind speeds at 700 mb. over the United States did not depart significantly from their normal values (fig. 2B). As a result the observed jet axes at 700 mb. bore a strong resemblance to their normal counterparts (not shown). Fast westerly flow prevailed across the Atlantic, where wind speeds were above normal in a narrow band centered around the 45th parallel (fig. 2). Greatest departures were observed in the eastern Atlantic, where speeds were as much as 6 m.p.s. above normal. Here also was found the center of greatest height anomaly over the Western Hemisphere, some 260 ft. below normal (fig. 1). Mean sea level pressures in this area were as much as 8 mb. below normal. A well-defined jet axis existed across the Atlantic (fig. 2A). This current split into two branches as it approached Europe, one branch passing northward through Scandinavia, the other southward across North Africa. Here again the configuration of the primary jet axes strongly resembled the normal.

The greatest anomaly of 700-mb. height, −310 ft., was associated with an extensive center of action over northern Asia (fig. 1). Very cold air, as much as 10° C. below normal in the layer from 1,000 mb. to 700 mb., accompanied this center. Because of this extreme cold, sea level pressures, on the average, were at most only 4 mb. below normal.

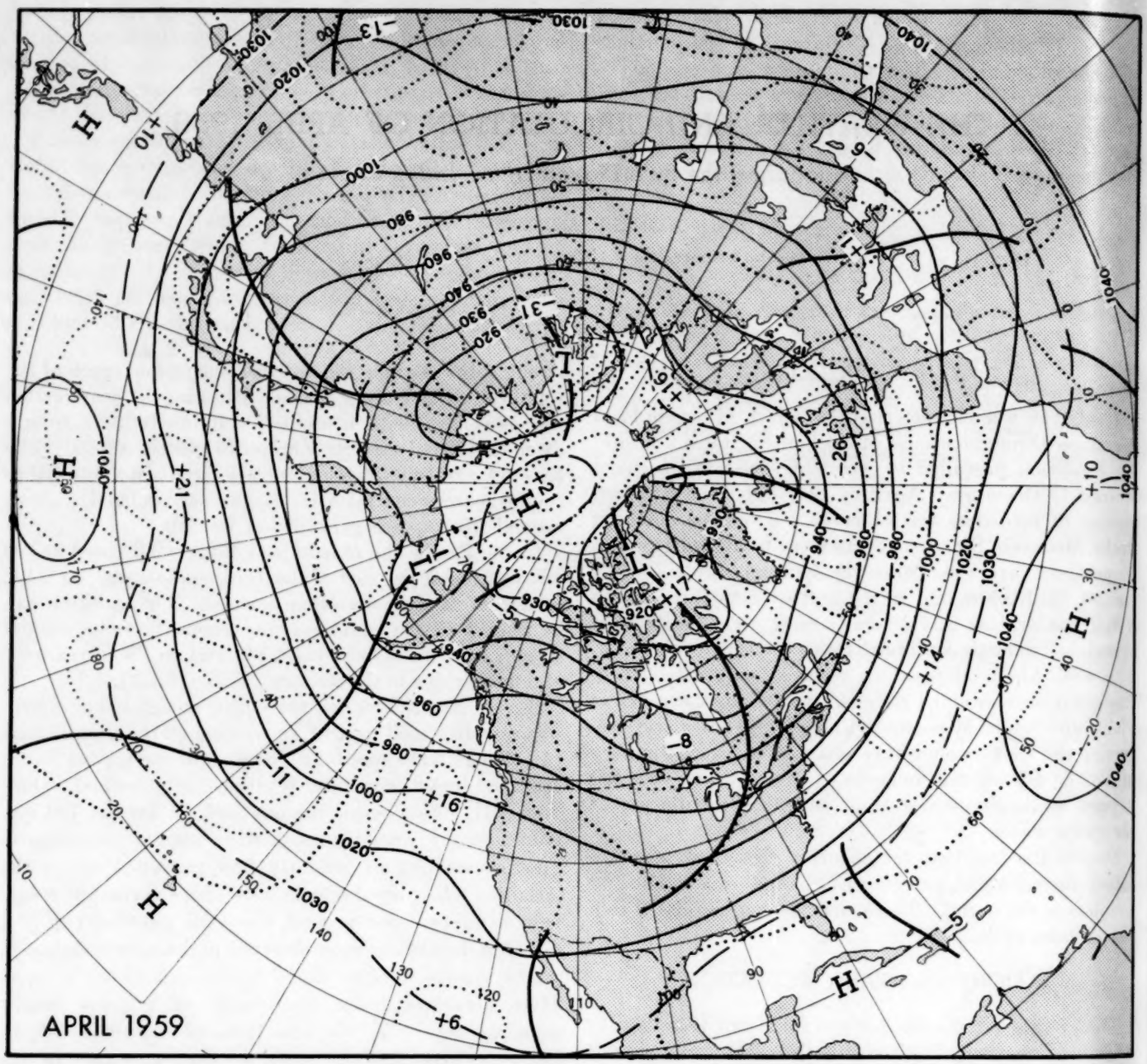

FIGURE 1.—Mean 700-mb. height contours (solid) and departures from normal (dotted) (both in tens of feet) for April 1959. Principal circulation features influencing weather in the United States were stronger than normal ridge near the west coast and trough in eastern North America.

3. AVERAGE UNITED STATES WEATHER RELATED TO THE MEAN CIRCULATION

Charts depicting the departure of average surface temperature from normal and the total precipitation for April are shown in figure 3. In addition, figure 4 gives the percentage of normal precipitation for April and for the period December 1958–April 1959.

A warm dry regime prevailed quite generally west of the Continental Divide, with temperature departures of

TABLE 1.—*Selected California cities which reported unusual warmth during April 1959*

City	Mean temperature (° F.)	Anomaly (° F.)	Years of record	Remarks
Burbank	65.0	+4.5	28	Warmest April of record.
Los Angeles (city office)	66.2	+4.7	82	
Los Angeles (airport)	65.4	+6.2	28	
San Diego	64.7	+4.2	87	
San Francisco (airport)	59.8	+5.7	31	
Oakland	60.1	+4.5	31	
Sacramento	64.3	+5.1	82	2d warmest April of record.
Blue Canyon	51.8	+6.7	54	

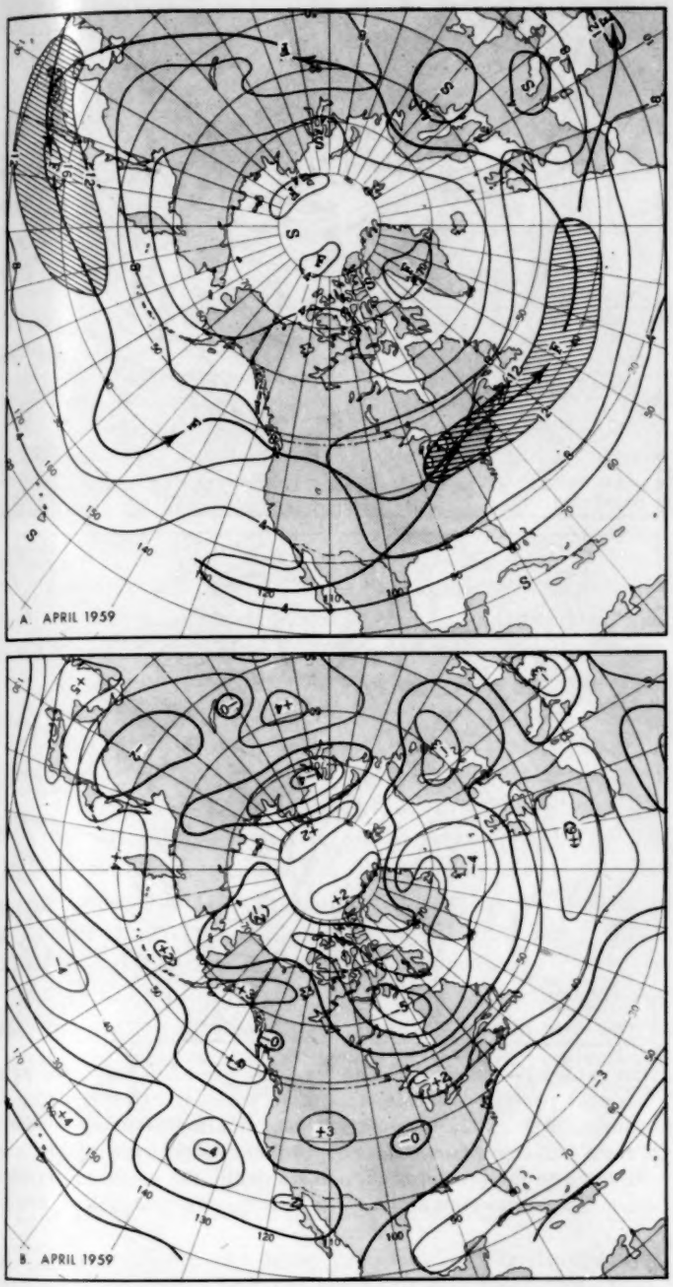

FIGURE 2.—(A) Mean 700-mb. isotachs and (B) departure from normal wind speed (both in meters per second) for April 1959. Solid arrows in (A) indicate primary axes of westerly jet, with speeds greater than 12 m.p.s. stippled. Jet maxima were located near the Asiatic coast and over the Atlantic Ocean, while wind speeds were close to normal over most of the United States.

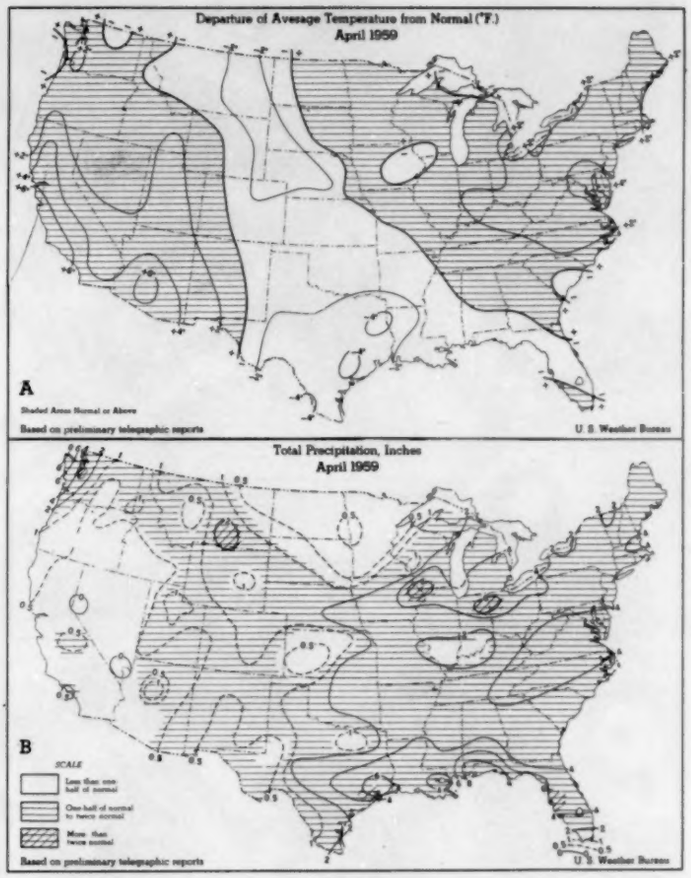

FIGURE 3.—(A) Departure of average surface temperature (° F.) from normal and (B) total precipitation (inches) for April 1959. Features were the record warmth along the California coast and continued precipitation deficiency in the northern Plains. (From *Weekly Weather and Crop Bulletin, National Summary*, vol. XLVI, No. 18, May 4, 1959.)

as much as 6° F. in portions of Arizona and California (fig. 3A). In the latter State the warmth was of a record-breaking nature, thus continuing the long period of unusual warmth which began during winter 1957–1958. Table 1 shows a representative list of cities in California where heat records were approached or established. Precipitation was markedly deficient throughout much of the Far West, with approximately 25 percent of normal in California, Nevada, southern Idaho, and western Arizona (fig. 4A). Since December 1958 a vast area from central Texas to southern California has received less than half its normal amount of precipitation (fig. 4B). Amarillo and Wichita Falls, Tex., have been drier than normal for 9 consecutive months. Abundant sunshine accompanied the warm, dry weather, with Ely, Nev., and Sacramento, Calif., experiencing their sunniest April on record.

Anticyclonic conditions associated with a stronger than normal upper-level ridge near the west coast (fig. 1) were largely responsible for this warm, dry regime. Moreover, northerly anomalous flow tended to inhibit precipitation. In California stronger than normal northeasterly flow resulted in foehn warming, thus contributing further to the unusual warmth along the coast.

Temperatures averaged below normal in the Great Plains, the lower Mississippi Valley, and along the Gulf coast (fig. 3A). Greatest departures were observed in southeastern Texas and northwestern Louisiana, where

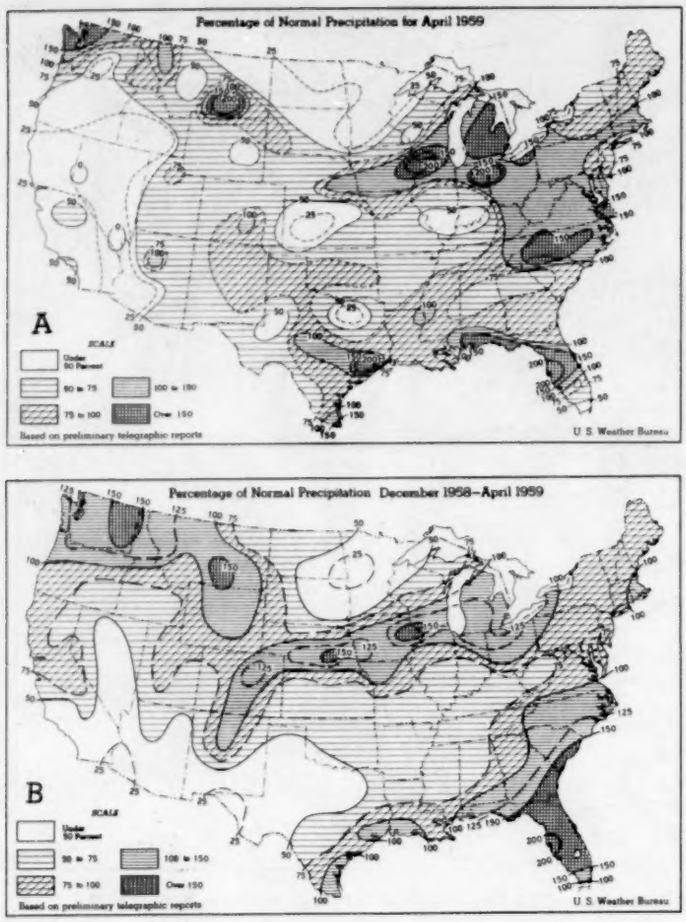

FIGURE 4.—Percentage of normal precipitation for (A) April 1959 and (B) December 1958–April 1959. Note prolonged period of dryness in Southwest and northern Plains. (From *Weekly Weather and Crop Bulletin National Summary*, vol. XLVI, No. 18, May 4, 1959.)

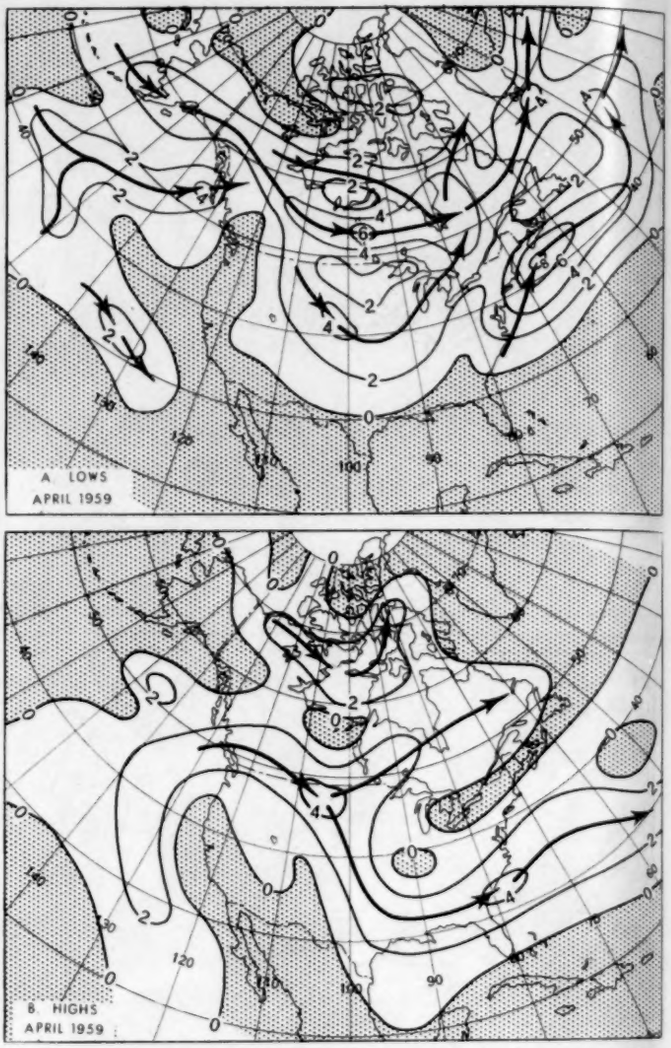

FIGURE 5.—Frequency of (A) cyclone passages and (B) anticyclone passages (within equal area boxes of 66,000 n. mi.^{2} [6]) during April 1959. Primary tracks are indicated by solid arrows. Cyclone tracks in the United States were rather well related to the precipitation pattern, while the major anticyclone track was associated with cool weather in mid-United States.

temperatures were as much as 4° F. below normal. Most of this coolness can be related to polar air masses associated with anticyclones steered southward by stronger than normal northerly flow (fig. 1) along a well-defined primary track (fig. 5B).

Precipitation in the Great Plains and Mississippi Valley was generally well below normal (fig. 4A). A large area in the Dakotas and Minnesota received less than a half inch of moisture during April (fig. 3B). In that area the total precipitation for the 5-month period December 1958 to April 1959 has been much below normal (fig. 4B). At Duluth and St. Cloud, Minn., with 1.34 and 1.22 inches for the period January to April, it was the driest such period in their respective 88 and 54 years of record. At Huron, S. Dak., this same period was the second driest in 77 years.

Most of this precipitation deficiency in the Plains States and Mississippi Valley appears to have been a function of stronger than normal northwesterly flow to the rear of the mean trough in eastern North America (fig. 1). In addition, the primary storm tracks passed both north and south of the northern Great Plains and upper Mississippi Valley (fig. 5A). Along the southern track a narrow band of heavier precipitation extended from southern Montana through Nebraska to the lower Lakes Region (figs. 3B and 4A). In Wyoming and Colorado, precipitation was largely in the form of snow which occurred during two periods and brought the month's total snowfall generally well above average. Heavy precipitation also occurred along the Texas coast, mostly as the result of overrunning of cool polar air masses in southwesterly flow aloft.

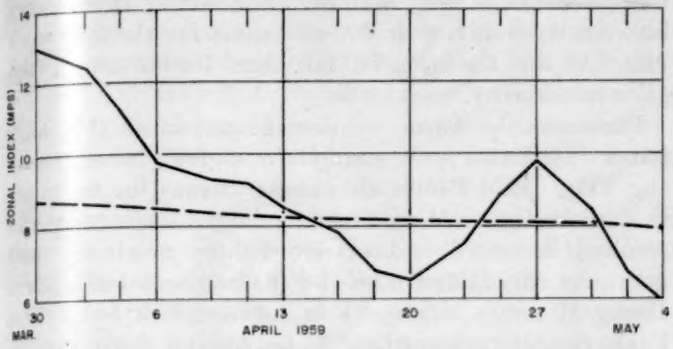

FIGURE 6.—Time variation of speed of 700-mb. westerlies averaged over the Western Hemisphere between latitudes 35° N. and 55° N. Solid line connects 5-day mean index values (plotted at middle of period and computed thrice weekly), while dashed line gives the corresponding normal. Index cycle was a prominent feature of the circulation.

Above-normal temperatures prevailed quite generally east of a line from the central Dakotas to southern Georgia, with greatest departures in the Middle Atlantic States (fig. 3A). This unseasonable warmth was associated with above normal heights and southerly anomalous flow at 700 mb. (fig. 1) and at sea level (chart XI in [5]). The heaviest precipitation in the United States occurred rather generally throughout the eastern half of the Nation (fig. 3B) and was related primarily to the mean trough (fig. 1). At sea level two principal storm tracks, one across the Great Lakes and the other along the Atlantic coast (fig. 5A), contributed to this precipitation. Lakeland, Fla., reported an alltime April precipitation record of 8.48 inches, with the January–April total of 28.00 inches also a record for the period. A relatively short distance away, Key West, Fla., with a long station record, received no measurable precipitation, also an April record. This extreme difference between Lakeland and Key West cannot readily be explained by large-scale, time-averaged charts.

4. WEEK-TO-WEEK VARIABILITY

Figure 6 shows the time variation of the temperate-latitude 5-day mean zonal index for April 1959. The complete index cycle portrayed here was accompanied by pronounced changes in weather and circulation. These changes will be described, using a series of 5-day mean 700-mb. charts centered 1 week apart, along with accompanying charts of weekly temperature departure from normal and total precipitation (figs. 7 to 11).

WEEK ENDING APRIL 5

The month began with the westerlies at their greatest strength, some 4 m.p.s. above normal (fig. 6), with fast flow predominating over nearly the entire hemisphere (fig. 7A). The only exception to this strong circumpolar whirl was in Europe, where a strong blocking ridge, accompanied by a Low in the Mediterranean, resulted in a

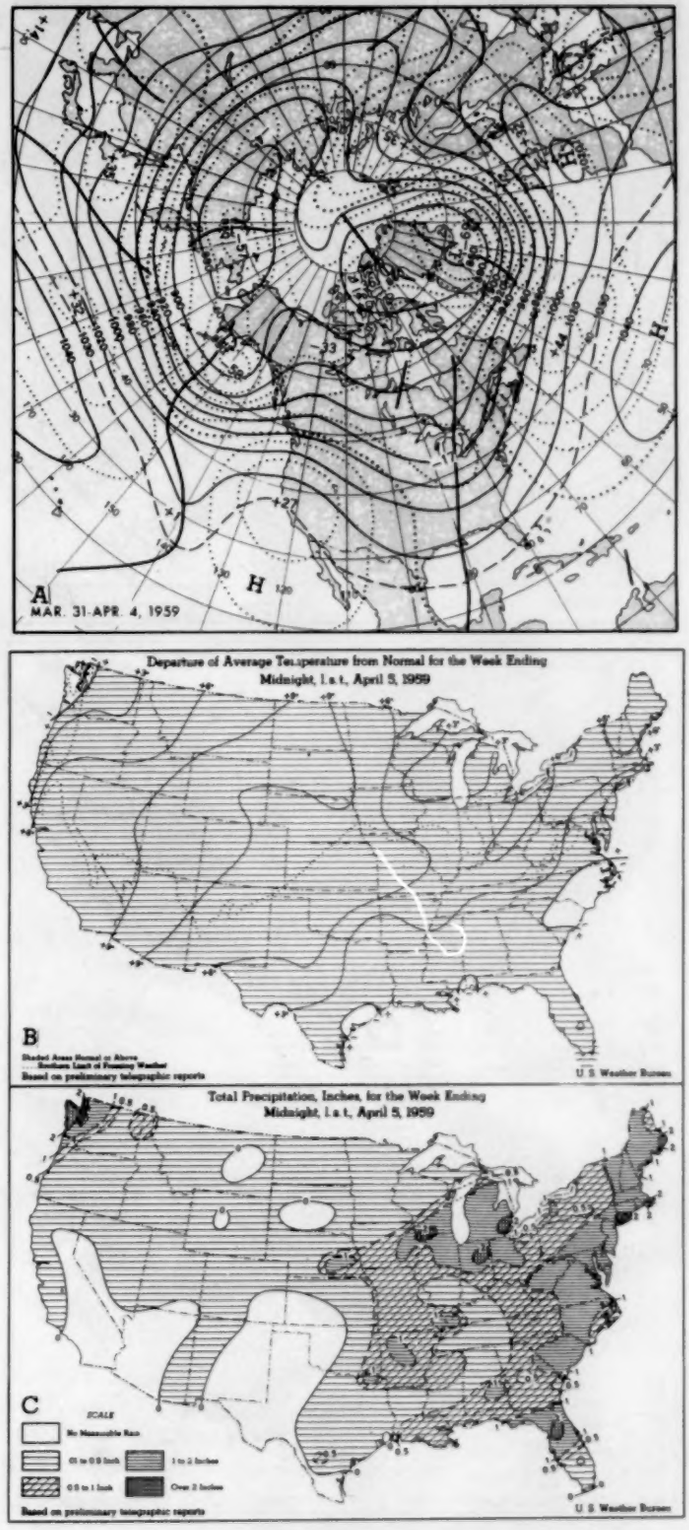

FIGURE 7.—(A) 5-day mean 700-mb. contours (solid) and height departures from normal (dotted) (both in tens of feet) for March 31–April 4, 1959. (B) Departure of average temperature from normal (° F.), and (C) total precipitation (inches) for week ending April 5, 1959. (B and C from *Weekly Weather and Crop Bulletin, National Summary*, vol. XLVI, No. 14, April 6, 1959.)

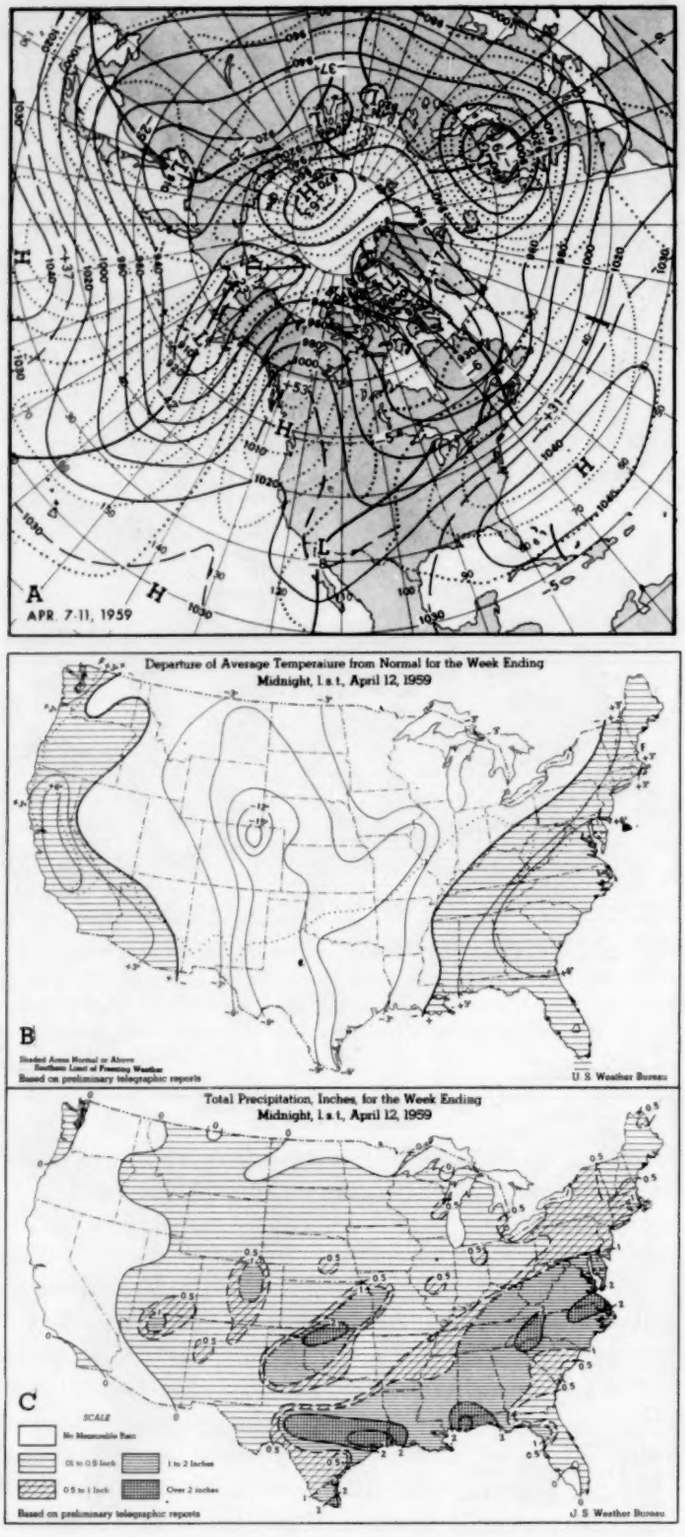

FIGURE 8.—(A) 5-day mean 700-mb. contours (solid) and height departures from normal (dotted) (both in tens of feet) for April 7–11, 1959. (B) Departure of average temperature from normal (° F.), and (C) total precipitation (inches) for week ending April 12, 1959. (B and C from *Weekly Weather and Crop Bulletin, National Summary*, vol. XLVI, No. 15, April 13, 1959.)

more meridional flow pattern. The strong resemblance between the 5-day mean 700-mb. chart for the first week (fig. 7A) and the mean 700-mb. chart for the month (fig. 1) is noteworthy.

Unseasonably warm weather accompanied this high index circulation over nearly the entire United States (fig. 7B). Mild Pacific air masses, warmed by foehn action in the Rocky Mountains, dominated the country and resulted in record or near-record daily maximum temperatures throughout much of the northern and central Rocky Mountain States. For instance, Salt Lake City, Utah, reported a record 82° F. on April 5, while Pueblo, Colo., with 83° F. on the 2d, equaled its previous April record.

Precipitation during the first week was confined mostly to the extreme Northwest and the area from the middle and lower Mississippi Valley eastward (fig. 7C). Most of the latter precipitation was associated with the deep trough in the Ohio Valley (fig. 7A) and fell as a deepening storm moved northeastward from the lower Great Plains (chart X in [5]). Tornadoes on the 2d caused some loss of life and extensive damage in northeastern Texas.

WEEK ENDING APRIL 12

Gradual amplification of the circulation pattern occured during the second week as the westerlies diminished to more normal values (fig. 6). In the mid-Pacific a stronger than normal ridge appeared, while farther east the mean trough of the previous week deepened while remaining nearly stationary (figs. 7A and 8A). Greatest changes occurred in North America, where strong ridging and a large area of positive height anomaly developed along the Pacific Coast (fig. 8A). At the same time the trough in eastern North America sheared, the higher latitude portion moving eastward, while the low-latitude portion retrograded and redeveloped in the Southwest. Blocking began to appear in the North Atlantic as an intense cyclonic center of action shifted from the eastern Greenland coast to the North Sea, thus replacing the strong ridge of the week before (figs. 7A and 8A). This rapid change in circulation was accompanied by an equally sharp change in weather throughout western Europe—from sunny and pleasant to cold and stormy. Blocking also appeared in the polar regions in the form of a high pressure area with 700-mb. heights as much as 630 feet above normal.

In the United States the change in circulation brought a rapid return to winter weather over much of the Nation. Stronger than normal northerly flow (fig. 8A) deployed very cold polar air into the United States, where temperatures for the week averaged well below normal from the Rocky Mountain States to the Ohio Valley—as much as 15° F. below normal at Denver, Colo. (fig. 8B). The cold was ushered in on the heels of a deep Alberta-type disturbance whose strong winds created severe dust storms

in the Dakotas, Minnesota, and Wisconsin on the 6th and 7th. Many new daily minimum temperature records were established by the abnormal cold in the northern and central Rockies, where only a few days before record warmth had prevailed. Some of these records were (in °F.): 12° at Helena, Mont., on the 9th; 7° at Denver, Colo., on the 10th and 12th; and 6° at Pueblo, Colo., on the 10th. In addition, a temperature of −3°F. at Cheyenne, Wyo., on the 12th was the coldest ever observed there so late in the season. The Far West and the East, where 700-mb. heights were above normal (fig. 8A), continued warm (fig. 8B). The period of greatest warmth in the East, from the 7th to 9th, saw numerous daily maximum temperature records established from Kentucky to southern New England. Baltimore, Md., reported the highest temperature, 92° F., on the 9th.

Precipitation was mostly moderate from Texas northeastward, with little or none over the Far West and northern Great Plains (fig. 8C). Snows were frequent over the Rocky Mountains and extended from the Texas Panhandle to the western Great Lakes. Over a foot of snow fell at the higher elevations in Wyoming and Colorado. Rains were rather persistent in Texas, with heaviest amounts along the upper coast (fig. 8C). The gradual eastward push of the cold air was accompanied by up to 6 inches of snow in parts of West Virginia, Maryland, and Pennsylvania on the 12th. The 6-inch fall at Charleston, W. Va., was the greatest snowfall ever recorded there in April.

This precipitation pattern was the result mostly of overrunning of cold polar air by warmer, more moist, tropical air in southwest flow aloft (fig. 8A). At sea level, high pressure dominated the North American continent, with easterly winds prevailing across most of the United States. The polar front lay in a nearly stationary position from the Middle Atlantic States to the western Gulf of Mexico for nearly the entire week.

WEEK ENDING APRIL 19

The westerlies continued to diminish, with their average strength below normal during this period (fig. 6). At 700 mb. the planetary circulation pattern assumed many of the characteristics commonly associated with a low zonal index. These include a relatively short wave spacing between trough-ridge systems, amplification, and increased cellular nature of the pattern (fig. 9A). The latter feature, which also characterizes blocking, is further illustrated by the 700-mb. height anomaly field. Note (fig. 9A) the preponderance of positive anomaly at higher latitudes and negative anomaly at lower latitudes over much of the Western Hemisphere.

The trough near the Asiatic coast moved eastward during the week, while retrogression of the ridge in western North America to the Gulf of Alaska cut off the eastern Pacific trough and limited it to a deep system

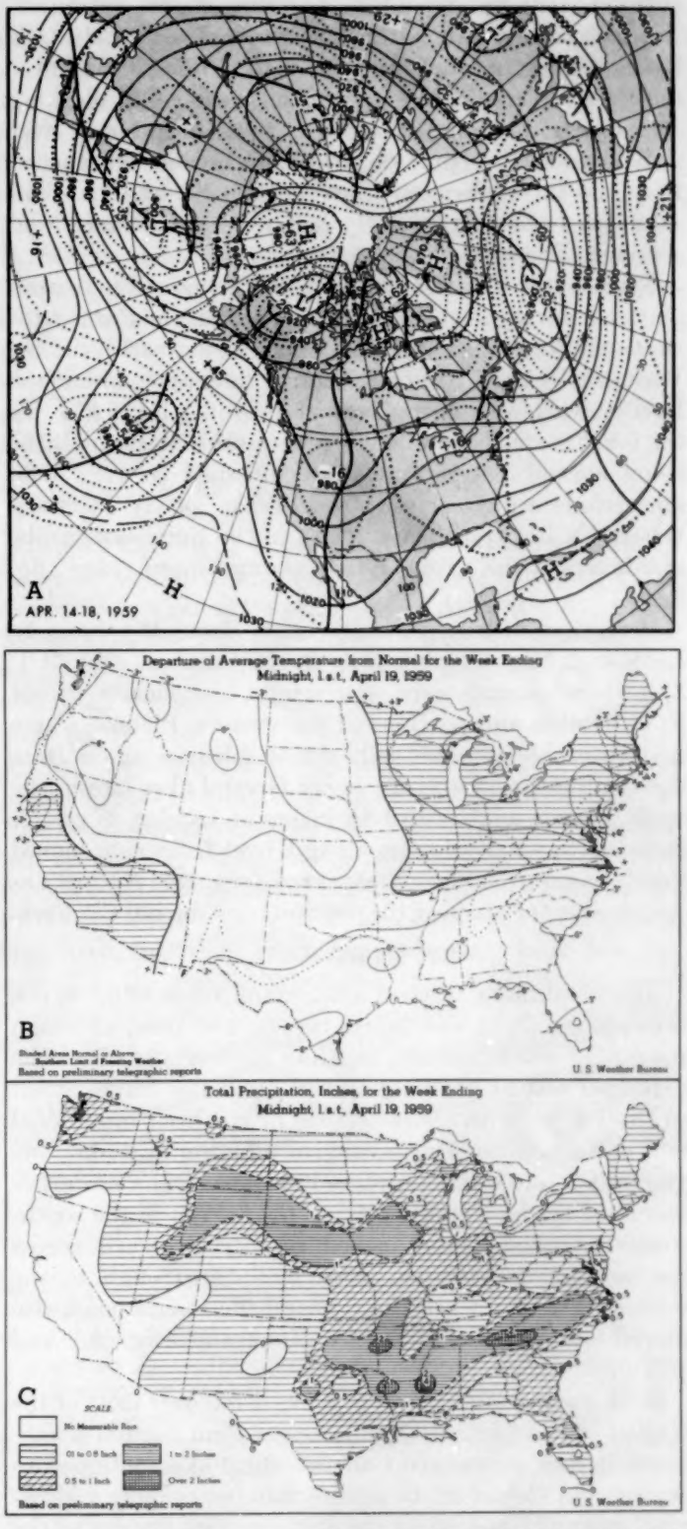

FIGURE 9.—(A) 5-day mean 700-mb. contours (solid) and height departures from normal (dotted) (both in tens of feet) for April 14–18, 1959. (B) Departure of average temperature from normal (° F.), and (C) total precipitation (inches) for week ending April 19, 1959. (B and C from *Weekly Weather and Crop Bulletin, National Summary*, vol. XLVI, No. 16, April 20, 1959.)

at lower latitudes (fig. 9A). As a consequence, retrogression also occurred in North America, where a nearly-full-latitude trough appeared in the West, while ridging over the East replaced a strong confluence zone. As blocking spread westward and southward from its position over polar regions the previous week, it became entrenched from the Davis Strait to Europe (figs. 8A and 9A) and suppressed the fast westerly belt over the Atlantic and southern Europe.

Temperatures in the United States remained unseasonably cool during the third week over all but the Far Southwest and Northeast (fig. 9B). The cool weather in the West was related to northwesterly flow aloft along the Pacific coast and below normal heights (fig. 9A). In the Gulf States, where heights were close to normal, the below-normal temperatures accompanied a very cold anticyclone which moved from Texas slowly eastward (chart IX in [5]). The warmth in the Northeast can be attributed to the stronger than normal mean ridge (fig. 9A).

Precipitation was generally heavy from Wyoming to Iowa and from Oklahoma to North Carolina (fig. 9C). Elsewhere amounts were mostly light to moderate, except in California and portions of the western Plateau where no measurable amounts fell. Snow fell once again from the Central Rockies to the lower Great Lakes late in the week, with a total fall of 15 inches at Lander, Wyo. A series of waves developing along a cold front as it moved slowly eastward and southeastward across the Nation was responsible for much of the precipitation during the week.

WEEK ENDING APRIL 26

The zonal index reached a minimum value of 6.5 m.p.s. between the third and fourth weeks, and then, although remaining below normal, began to recover (fig. 6). The principal seat of blocking spread from the Davis Strait to the Pacific with characteristic pronounced meridional flow pattern, strong ridges, and cut-off lower latitude Lows (fig. 10A). As blocking relaxed in Canada, the westerlies increased across North America, the trough in the southwestern United States moved rapidly eastward across the country and amalgamated with the trough in the western Atlantic, while the ridge off the Pacific coast also moved eastward to the Rocky Mountains (figs. 9A and 10A).

Subnormal temperatures predominated over most of the United States (fig. 10B) as stronger than normal northwesterly flow in western Canada (fig. 10A) continued to deploy cold Canadian air masses into the country. However, eastward motion of the trough-ridge system in the United States was related to a warming trend which gradually spread eastward. This is readily seen by comparing figure 9B with figure 10B. Note the growth of the area of above normal temperatures in the Far West, associated with ridging and above normal heights, and the diminu-

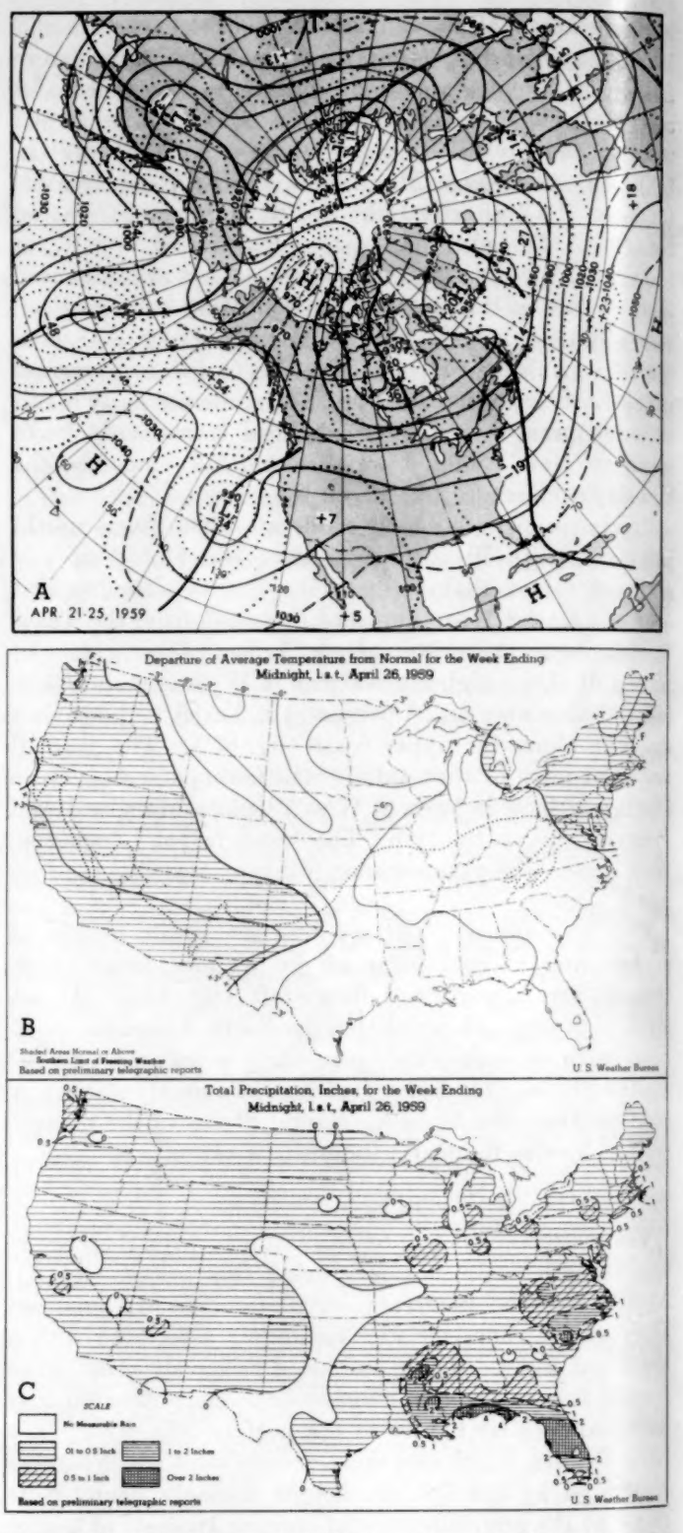

FIGURE 10.—(A) 5-day mean 700-mb. contours (solid) and height departures from normal (dotted) (both in tens of feet) for April 21–25, 1959. (B) Departure of average temperature from normal (° F.), and (C) total precipitation (inches) for week ending April 26, 1959. (B and C from *Weekly Weather and Crop Bulletin, National Summary*, vol. XLVI, No. 17, April 27, 1959.)

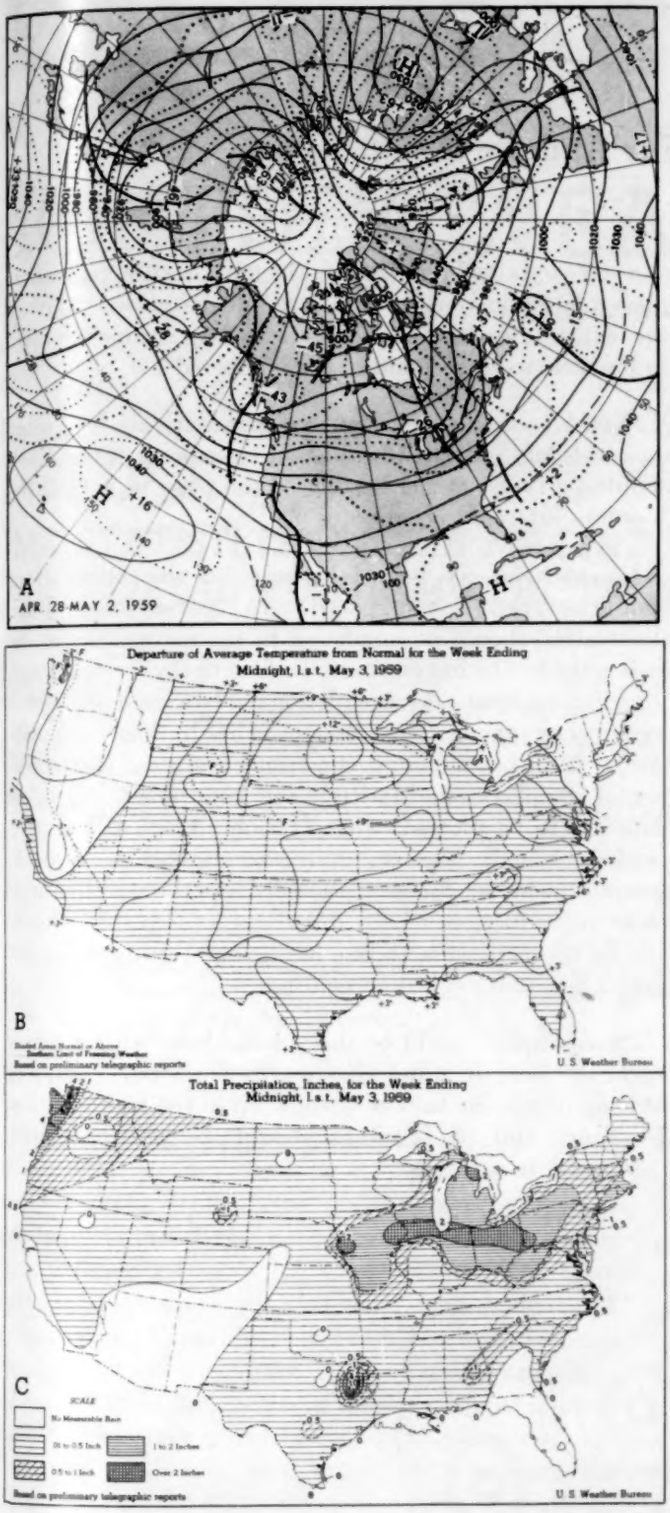

FIGURE 11.—(A) 5-day mean 700-mb. contours (solid) and height departures from normal (dotted) (both in tens of feet) for April 28–May 2, 1959. (B) Departure of average temperature from normal (° F.), and (C) total precipitation (inches) for week ending May 3, 1959. (B and C from *Weekly Weather and Crop Bulletin, National Summary*, vol. XLVI, No. 18, May 4, 1959.)

tion of the area of above normal temperature in the Northeast, related to the decrease in 700-mb. height (figs. 9A and 10A). At Roswell, N. Mex., the temperature reached 97° F. on the 25th, an April record.

The precipitation pattern also tended to move eastward from the preceding week (figs. 9C and 10C). Heaviest amounts fell in the eastern Gulf States and portions of the Atlantic Coastal States. Most of this occurred early in the week in connection with a cold front and cyclonically curved contours at 700 mb. (fig. 10A). As the west coast ridge moved inland and the eastern Pacific trough approached the coast, precipitation broke out in California, southern Oregon, and western Nevada. Rain on the 25th at Burbank, Calif., ended a period of 62 consecutive days without measurable precipitation.

WEEK ENDING MAY 3

A peak value of 9.6 m.p.s. was reached by the zonal index between the fourth and fifth weeks, thus completing the cycle which began at the beginning of April (fig. 6). This increase in the mid-tropospheric zonal circulation was manifested at the 700-mb. level by eastward motion of nearly all the mean trough and ridge systems (figs. 10A and 11A).

The warming trend in evidence in the West the previous week overspread almost the entire country, with only the Northwest and extreme Northeast experiencing below normal temperatures (fig. 11B). Greatest departures were reported in the middle of the Nation, where a large anomaly area greater than +9° F. was observed. Heavy precipitation, the result of strong onshore cyclonic flow, returned to the Pacific Northwest (fig. 11C), while heavy amounts were also reported from Iowa to southern New England as a by-product of the trough over the Great Lakes (fig. 11A).

April came to a close with the westerlies decreasing rapidly, and as May began they were once again well below normal (fig. 6).

REFERENCES

1. P. Stark, "The Weather and Circulation of April 1958," *Monthly Weather Review*, vol. 86, No. 4, Apr. 1958, pp. 132–140.
2. J. F. Andrews, "The Weather and Circulation of April 1957—A Stormy Month Over the United States Characterized by Two Contrasting Temperature Regimes," *Monthly Weather Review*, vol. 85, No. 4, Apr. 1957, pp. 124–131.
3. J. F. O'Connor, "The Weather and Circulation of February 1959," *Monthly Weather Review*, vol. 87, No. 2, Feb. 1959, pp. 81–90.
4. U.S. Weather Bureau, "Normal Weather Charts for the Northern Hemisphere," *Technical Paper* No. 21, Washington, D.C., Oct. 1952, 72 pp.
5. U.S. Weather Bureau, *Climatological Data, National Summary*, vol. 10, No. 4, April 1959, charts IX–XI.
6. E. M. Ballenzweig, "A Practical Equal-Area Grid," *Journal of Geophysical Research*, vol. 64, No. 6, June 1959, pp. 647–651.

Suggestions For Authors

Articles are accepted for the *Monthly Weather Review* with the understanding that they have not been published or accepted for publication elsewhere.

Two copies of the *manuscript* should be submitted. All copy, including footnotes, references, tables, and legends for figures, should be double spaced with margins of at least 1 inch on sides, top, and bottom. Some inked corrections are acceptable, but pages with major changes should be retyped. The style of capitalization, abbreviations, etc., used in the *Review* is governed by the rules set down in the Government Printing Office Style Manual.

Tables should be typed, each on a separate page, with a title provided. They should be numbered consecutively in arabic numerals.

In *equations*, conventional symbols in accordance with the American Standards Association Letter Symbols for Meteorology should be used. If equations are written into the manuscript in longhand, dubious-looking symbols should be identified with a penciled note.

References should be listed on a separate sheet numbered in the order in which they occur in the text; or, if there are more than 10, in alphabetical order according to author. The listing should include author, title, and source (if the source is a magazine, the volume, number, month, year, and complete page numbers should be listed; if the source is a book, the publisher, place and date of publication, and the page numbers of the reference). If reference is made to a self-contained publication, the author, title, publisher, place of publication, and date should be given. Within the text, references should be indicated by Arabic numbers in brackets to correspond to the numbered list.

Footnotes should be numbered consecutively in Arabic numerals and indicated in the text by superscripts. Each should be typed at the bottom of the page on which the footnote reference occurs.

Illustrations.—A list of legends for the illustrations should be typed (double spaced) on a separate sheet. Each illustration should be numbered in the margin or on the back outside the image area. To fit into the *Review* page, illustrations must take a reduction not to exceed 3½ inches by 9 inches (column size) or 7½ inches by 9 inches (page size). Map bases should show only political and continental boundaries and latitude and longitude lines, unless data are to be plotted, when station circles will also be needed. Usually the less unnecessary detail in the background the better will be the result from the standpoint of clear reproduction. Line drawings and graphs should also be uncluttered with fine background grids unless the graph demands very close reading.

Photographs should be sharp and clear, with a glossy surface. Bear in mind that marks from paper clips or writing across the back will show up in the reproduction. Drawings and photographs should be protected with cardboard in mailing.

U. S. GOVERNMENT PRINTING OFFICE: 1950